Faculty of Natural Science and Technology
Department of Physics

NTNU
Innovation and Creativity

MASTER'S THESIS FOR

STUD. TECHN. [BÅRD MARTIN KJELLING]

Thesis started: [21.01.2008]
Thesis submitted: [04.08.2008]

DISCIPLINE: [PHYSICS]

Norsk tittel: *"Orden og uorden av vanninterkalerte tilstander i fluorhektorittleire"*

English title: *"Order and disorder of water intercalated states in fluorohectorite clay"*

This work has been carried out at the laboratory for soft and complex matter studies at the department of Physics, under the supervision of Jon Otto Fossum

---

Trondheim, 04.08.2008

Jon Otto Fossum

Responsible supervisor

Professor at Department of Physics

Abstract

Water intercalated states in NaFH have been mapped in an experiment varying the relative humidity around a powder sample. The phase transition from the one water layer(1WL) hydration phase to the two water layers(2WL) phase, and in the other direction was measured as d-spacings of the layered particles changed. A hysteresis curve was found with transition temperature and hysteretic width equal within error margines to an identical experiment on the same sample done at a lower temperature. Indications from the phase transition curve, and the diffraction profiles inbetween strongly bounded 1WL and 2WL intercalated states show that the 2WL and 1WL states are likely the only predominating states of crystalline-like bonding within all humidities except the lowest.

For studying ramdomly intercalated states a synchrotron source was utilized to achieve small beam sizes while still having useful intensities for measurements. It was found that Hendricks-Teller signatures were very sensitive to the configuration of the intercalation front. More specifically it seemed to depend on the width of the intercalation front or the relative magnitude of the humidity gradient, i.e. humidity difference divided by length. Some hypotesis are presented to try to make account for new findings in NaFH.

A Wide Angle X-ray Scattering(WAXS) was done at the Complex lab at NTNU with a two-dimensional detector. Diffraction profiles were gathered having qualitatively good agreement to diffraction profiles previously gathered for very similar samples. The spatial resolution was however far from as good as conventional one-dimensional wide angle diffractometers and at moderate diffraction angles measurable peak shifts ensued from sample broadening effects. Diffraction profiles for NiFH changing both the relative humidity and the temperature of the sample was gathered and compared. Temperature did not seem to matter for the d-spacing, but the effectively changing humidity inside the sample chamber produced relatively small, but discernible shifts in d-spacings. A peak, not identified within the group previously, varied characteristics as d-spacings changed in the course of the experiment, and this is hypothesized as being related to a peak of the interlayer water bound to the Nickel-cation or the clay surface.

Preface

The experiments presented in this master's thesis was done during one semester at the division of complex materials at NTNU. A synchrotron source was utilized in an experiment done in Pohang, Korea at the Pohang Accelerator Laboratory(PAL). It has been inspiring to be "hands on" with all research equipment and experimental designs during the work.

The synthesis of theoretical models to fit observed behavior of Nature, lies at a kernel of physics and being an active, though small, contributor in such a process gives much satisfaction and gives incentives to delve deeper into understanding the fundamental laws governing nature.

Clays have been used by humans as long as we have evidence of human civilization. Today they still get used for the same things that they have been used for, but clay is rapidly finding new fields of usage, and there does not seem to be deficiencies in potential uses for it. Novel uses include sensor technology, catalysis and impermeable barriers such as for instance in a landfill liner.

In this report focus has primarily been on different states of water intercalation in two synthetic clays, namely Sodium-Fluorohectorite(NaFH), and Nickel-Fluorohectorite(NiFH) using the probe of X-rays.

Acknowledgements

An attempt to make humoristic thanks to the people contributing to the success of the experiments does hopefully not make the mentioned or not mentioned people feel belittled of the serious efforts they have made.

First I would like to express gratitude to my skilled supervisor Jon Otto Fossum whom I could always trust to be engaged in my progresses, even when it meant doing trivial stuff such as solving Bragg's law. Big thanks to Kim Chan, a masterstudent at GIST, Korea, for *not* giving the details on how the synchrotron's diameter was some millimeters(!), and once in a while also himself ask a silly or naive question. Thanks to Do Young Noh, professor at GIST, for taking us out for Korean meat before it was too late. Thanks to, Yavuz Öztürk, Ph.D. student at GIST, for bringing some dynamics into our lives at the synchrotron. I am indebted to Elisabeth Lindbo Hansen,

fellow masterstudent, not least for helping some of my poor Yorick-formats be converted and live again. I thank Ole Tore Buset, sectional engineer, for showing me the ON button when it mattered most and bumping the X-ray source providing an intensity boost. Many thanks goes to the workshop at NTNU for making my design drawings look rather inferior to the products made. Thanks go also of course to Romulo P. Tenrio, Ph.D. student, for collaboration on the phase transition experiment, making important suggestions, but being correct in a discreet and gentleman fashion. Yves Meheust, an associate professor in France, who invariably had a right fit. Lars Ramstad Alme, a previous master student, for giving pointers, and answers to questions but not providing a recipe on how the filling of capillaries were to be done the "right" way. I finally thank Kim Magnus, fellow masterstudent, for boosting moral with puzzling intellectual problems but always providing definite *answers* to them.

Contents

1 Theory **6**
- 1.1 Clay minerals . . . 6
  - 1.1.1 Smectite clays and structure of fluorohectorite . . . 8
- 1.2 X-Ray Scattering . . . 9
  - 1.2.1 Creation and scattering of X-Rays . . . 9
  - 1.2.2 Scattering of X-Rays and diffraction . . . 10
  - 1.2.3 Intercalation in Clay Minerals . . . 16
  - 1.2.4 Peak Characteristica and fitting with Pseudo-Voigt function . . . 17
  - 1.2.5 Random intercalation states - Hendricks-Teller formulation . . . 18
- 1.3 Hydration phase transitions . . . 19

2 Experimental section **21**
- 2.1 Hydration phase transition . . . 21
  - 2.1.1 Experiment design . . . 21
  - 2.1.2 Experimental equipment . . . 22
  - 2.1.3 Control, data collection and uncertainty . . . 25
  - 2.1.4 Method of analysis . . . 27
- 2.2 Mixed water intercalation states in NaFH . . . 28
  - 2.2.1 Experiment design . . . 28
  - 2.2.2 Experimental equipment . . . 28
  - 2.2.3 Uncertainty and data collection . . . 29
  - 2.2.4 Method of analysis . . . 29
- 2.3 Fluorohectorite wide angle diffraction profile . . . 30
  - 2.3.1 Experiment design . . . 30
  - 2.3.2 Experimental equipment . . . 30
  - 2.3.3 Data collection and uncertainty . . . 32
  - 2.3.4 Method of analysis . . . 32

3 Results and discussion **33**
- 3.1 Phase transition . . . 33
- 3.2 Mixed intercalation states in NaFH . . . 35

3.3 Wide angle diffraction profile for fluorohectorite 40

4 Conclusions **47**

A X-Ray microscopy images of NaFH-particles **49**

Chapter 1

Theory

1.1 Clay minerals

"A mineral is a naturally occurring homogeneous solid with a definite chemical composition and a highly ordered atomic arrangement" [1]. Many clay mineral grains and particles have thus properties of similarity or even equivalency to crystals. Structure determination is therefore to a great extent achieved through methods applied in crystallography, and we will, after laying some of the foundation, soon move to the the structure of a particular kind of the smectite clays, namely fluorohectorite. A short outline of the paradigms in classification of clays and their fundamental building-blocks is given first.

Clays' fundamental building block consist of tetrahedral and octahedral sheets of mostly silica linked to oxygen atoms in the tetrahedras. The tetrahedra are corner-linked and the octahedra are edge-linked[2]. A semi-general model of a so-called 2:1 layered type of clay is shown in figure 1.1.

In figure 1.1(a) an interlayer cation in the interlayer space is represented. This will be attracted to the interlayer space and in effect neutralize the effect of the buildup of charges that results if for example Si^{4+} is substituted by Al^{3+} in the tetrahedral sheet or Li^{1+} substitute for Al^{2+}(as the case is for fluorohectorite) in the octahedral sheet. The negative charge will then seek neutralization by attracting a cation in(to) the interlayer space between the two silica sheets as in figure 1.1(a). In this figure we can clearly observe how the 2:1 layer types of clays are configured with the tetrahedral sheets the octahedral sheet - the top silica sheet being inverted to fit the octahedral sheet. There also exists 1:1 and 2:1+1[1] types and these different types is an important way in which one differentiates among the clay minerals.

The concept of layer charge is widely used to distinguish clay minerals. Substitution of lower valenced atoms in the tetrahedral and octahedral sheets, e.g. a lithium atom instead of a magnesium atom in the octahedral

[1] One extra octahedral sheet between the 2:1 layer with positive charge.

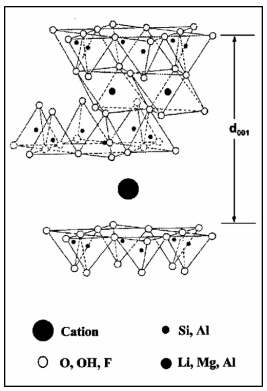

(a) Principial structure of a 2:1 layered clay mineral. From [3].

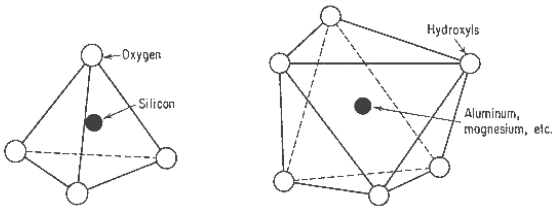

(b) Tetrahedron and octahedron building blocks of clay minerals.From [4].

Figure 1.1: The generic building blocks of 2:1 type clay minerals

sheet, will cause charge to accumulate on the faces of the layers. This charge is typically between 0 to -1e (but the group of Brittle micas can have -2e) per half-unit cell and will rarely be slightly positive. The charge is highly important in clay swelling, both in osmotic[2] and crystalline swelling[5]. Classifying clays depending on its layer charge is a standard practice in clay mineralogy. Layer charge is commonly measured in electrons per half-unit cell, and is roughly attributed or thought to distribute evenly on the surface of the tetrahedral sheet. The amount will vary from between -2e to no layer charge per half-unit cell or more rarely to have positive layer charge. The quantity of layer charge and its distribution will greatly influence a series of properties concerning interlayer adsorption (or if none exists, why not) and binding between layers.

Further one distinguishes between dioctahedral and trioctadral which corresponds to a brucite-like and a gibbsite-like sheet structuring respectively. This differentiates between cases where every third octahedral site in the octahedral sheet is unoccupied by the cation (most often Mg^{2+}), then called dioctahedral, or where every octahedral site is occupied (most often Al^{3+}) constituting the trioctahedral variant.

There are also more ways to distinguish amongst groups of clay minerals, noticably among them the species of the interlayer cation in the interlayer space.

The unit cell of fluorohectorite, and that of most clay minerals of Ver-

[2]The clay crystal particles have so much of water or organic molecules inbetween the layers it looses crystal integrity creating a diffuse electric double layer. This process can also be termed to be one of delaminating.

miculite and Smectites have a crystal system being monoclinic[3] For the fluorohectorite the direction of stacking of layers is normal to the tetrahedral sheet. The a- and b-axis of the crystal lies in the plane of this sheet. Values for the unit cell dimensions of a fluorohectorite [4] was found by Breu[23] to be $a = 5.26\,\text{Å}$, $b = 9.13\,\text{Å}$, $c = 13.98\,\text{Å}$ and $\beta = 96.89°$. Especially c will differ significally for the samples studied in this report.

1.1.1 Smectite clays and structure of fluorohectorite

Smectite clays have layer charge approximately between -0.2 to -0.6e The layer structure can either be 1:1 or 2:1. Smectites are characterised by their ability to intercalate organic molecules into their interlayer space, swelling and simultaneously keep their structural characteristics as well as the bonding between the layers. It is ergo maintaining its crystal integrity. As a consequence of this it is possible to observe different stacking distances or basal spacings of layers given by $d_{001} = c \cdot \sin\beta$.

Synthetic fluorohectorite have the following structural formula where R signifies the cation:

$$\mathbf{R}_y(\mathbf{Mg}_{3-x}\ \mathbf{Li}_x)\ \mathbf{Si}_4\mathbf{O}_{10}\mathbf{F}_2$$

For hectorite the fluorine atoms have substituted the hydroxyls in the octahedral sheet. For R to neutralize the negative charge caused by substitution of the magnesium atoms with lithium atoms we should have $y = x$ when R is monovalenced or $y = x/2$ when it has a valence of 2. For the monovalenced NaFH y is 0.6.

The presented material so far has been the idealized structures of the regular octahedrons and tetrahedrons joining together to form a unit cell structure. This description has been ignoring the interlayer material, which in most cases will not be bound to specific sites and is not properly crystalline. Including the material in the interlayer the decided upon term is the *unit structure*[5]. One distortion to the sheets has its origin from the joining of tetrahedral and octahedral sheets because of the different bonding lengths to the oxygen atoms from the atoms in the tetrahedral and octahedral sheets. Effects include *1)* thickening of the tetrahedral sheet, *2)* tilting the tetrahedra and *3)* rotating adjacent tetrahedrals towards or away from eachother in the plane made up of the oxygen atoms thereby disturbing or destroying the hexagonal form for the oxygen planes [2]. There are in addition to these groups of clay minerals the so-called polytypes which is a special type of polymorphism restricted to layered structures[2].

[3] In the monoclinic crystal system there are three different unit cell axis; two of the angles (α and β) are right angles while β is an obtuse angle[28].

[4] The fluorohectorite investigated was intercalated with a large cationic pillar from a previously Cs-intercalated fluorohectorite to create three-dimensionally ordered structures of true crystals.

1.2 X-Ray Scattering

1.2.1 Creation and scattering of X-Rays

X-rays are electromagnetic radiation or photons having a definite wavelength approximately between 0.01 to 10 Ångström(1Å =0.1nm). These X-Rays will with a probability scatter off the electrically charged clouds from atoms or molecules that they are in proximity of. The single interaction which makes the photon(or quantum of electromagnetic radiation if you will) scatter can in many cases be considered as semi-classical[5] elastic or inelastic scattering by two bodies with electric charge.

Creation of X-Rays

X-rays are produced by either acceleration or deceleration of charged particles. This will cause electromagnetic radiation from the charged particle. The most used source of X-rays around is still the Coolidge tube. This is a tube with an evacuated chamber with a cathode-anode to accelerate electrons from the cathode to the anode. There should exist a quite high voltage difference (typically 40kV) between them to accelerate them to the right energies. The anode of a certain metal release photons with a range of wavelengths but have peaks which is determined by the type of deexitations of electrons in a lower bound shell to a higher bound shell and typically then from the L-shell to the K-shell. These electron transitions have names according to which shell they go to and come from. The transition from the L- to K-shell is called a K_α transition. The emission spectrum of electromagnetic radiation for a typical anode tube is shown in figure 1.2.1. The features for most of the wavelengths except the sharp peaks are determined by what is called Bremsstrahlung. This is caused by the charges of electrons decelerating in the metal, giving out electromagnetic radiation.

The modern X-ray sources of synchrotrons utilizes acceleration instead of deceleration of charged particles to produce the X-rays. Historically synchrotron radiation was discovered in 1947[30] in a research laboratory of General Electric. There is now a considerable number of synchrotrons around the world. The big synchrotron facilities are located in America, Europe and Japan. A figure of merit for the quality of X-Ray sources is the brilliance or spectral brightness[25, 26]. This is defined as

$$B = \frac{\text{Number of incoming photons per second}}{\text{Optical source area}[\text{mm}^2] \cdot \text{ Beam divergence } [\text{mrad}^2] \cdot 0.1\% \text{ bandwidth}}. \tag{1.1}$$

The order of magnitude for the brilliance for a standard X-Ray tube is approximately 10^9 while synchrotron bending magnets have approximately a

[5] Relativistic mass for the two particles must be taken in account of.

brilliance of 10^{14} and an undulator[6] 10^{19}. To control the radiation and keep the brilliance of the source the electrons are stored in a circular path called a storage ring. The circular path keeps its radial acceleration by magnets which bend the electrons' trajectories by the Lorentz force.

There are different reasons for wanting a very high beam or electron energy. Firstly this will produce a radiation spectrum which reaches into the region of hard x-rays. Hard x-rays are those with smaller wavelengths and "sees" scales of interatomic distances well. But a further advantage for keeping the energy at a high level is that this will cause little beam divergence. For higher energies causes the electron paths to have very sharp directions, and thus creating very small opening angles for the beam[26].

Some formulas which will characterize a synchrotron's performance are given[26]. The radius of curvature for the beam ρ is given practically as

$$\rho = 3.32 \qquad \frac{E\,[\text{Gev}]}{B} \tag{1.2}$$

where B, the magnetic field of the bending magnets in the storage ring is given in Tesla. The critical frequency ω_c of the emission spectrum parts the spectrum such that half of the radiated power lies above and half below this frequency. The associated wavelength λ_c is

$$\lambda_c = \frac{4\pi}{3}\frac{\rho}{\gamma^3} \tag{1.3}$$

where γ is the Lorentz factor ($\sqrt{1/(1-v^2/c^2)}$). This can be rendered in more practical units, like

$$\lambda_c = \frac{18.64}{B\,[\text{Tesla}] \cdot E^2\,[\text{GeV}^2]}. \tag{1.4}$$

1.2.2 Scattering of X-Rays and diffraction

The photon can scatter elastically off the electron, not exchanging any energy or momentum, or there can be an inelastic interaction decreasing the momentum of the photon. The former is called Thomsom scattering, and the latter is most often Compton scattering where the interaction is electric repulsion between the electron and the photon.

Thomson scattering

In Thomson scattering the electromagnetic field will make the electron vibrate at the same frequency as the incoming radiation and will consequently

[6] An insertion device in synchrotrons using alternating magnetic fields across the electrons' trajectory, producing in effect a very bright, coherent and collimated source of X-Rays.

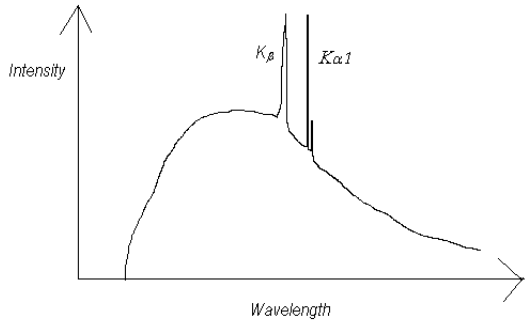

Figure 1.2: Electron transitions in a simplified schematics.

emit radiation spherically. The phase of the incoming radiation is in phase with the outgouing and the scattering is thus coherent. The intensity of the scattered radiation of one scatterer is [6]

$$I = \frac{1}{2}\left(\frac{e^2}{4\pi\epsilon_0 c^2 m}\right)^2 (1 + \cos^2 2\theta) I_0. \tag{1.5}$$

The quantities are the electric charge, the elecric permittivity, mass of scatterer, scattering angle, and incident intensity. This is known as Thomson's formula and is strictly valid only for free electrons and ignoring the magnetic interaction which is weak. When we consider scattering with atomic electrons we must handle it quantum-mechanically. Knowing the wave function for the electron we can determine the charge distribution by the relation $\rho = |\psi|^2$. Taking the Fourier transform[7] of this over all space gives the amplitude from the electron. Considering now an electron set at a point in the origin and looking only at a scattering of a certain magnitude (that implies that we are looking at monochromatic photons coming from one direction and scattering also happens only into one direction). We get, assuming the scattering for an atom will be spherical, for a given s a fraction of the total amplitude scattered from the electron and we denote this by p_s. We have that

$$p_s = 4\pi \int_{r=0}^{\infty} \rho(r) r^2 \frac{\sin(2\pi r s)}{2\pi r s} \mathrm{d}r. \tag{1.6}$$

An expression of the scattering factor of an atom was the objective and motive for doing this short and coarse derivation adopted from [6]. The scattering factor is the ratio of the amplitude of the coherent scattered radiation from an atom with Z electrons to that of one electron situated at the

[7] The component of the integral is $\exp(2\pi \mathrm{i}\, r\, s\, \cos\psi)$where s is the scattering vector.

atoms centre.

$$f_a = 4\pi \int_{r=0}^{\infty} \rho_a(r) r^2 \frac{\sin(2\pi rs)}{2\pi rs} \mathrm{d}r = \sum_{j=1}^{Z} (p_s)_j, \tag{1.7}$$

where $\rho_a(r)$ is the total charge density of the electrons in the atom.

Diffraction of X-Rays The unit cell structure factor is

$$F(hkl) = \sum_{i=1}^{n} f_i \exp(\mathrm{i}\mathbf{q} \cdot \mathbf{r_i}) \tag{1.8}$$

where we have n atoms in the unit cell and attribute the scattering to originate in the atom's center. $\mathbf{q}$ is defined

$$\mathbf{q} = \mathbf{k}_{scattered} - \mathbf{k}_{incoming} \tag{1.9}$$

With $|\mathbf{k}_s| = |\mathbf{k}_i|$ (elastic scattering) equal, and looking a moment at figure 1.2.2 to find that the angle between this two vector is 2θ, this gives

$$q = \frac{4\pi \sin(2\theta/2)}{\lambda} \tag{1.10}$$

Returning to the structure factor, the indices hkl are those for reflection which also are the Miller indices for the reciprocal basis vectors(a^*, b^*, c^*). The structure of the crystal will determine which reflection which we can expect. If we consider planes of the crystal with atoms equispaced from eachother in both directions, atoms acting as point scatterers, the waves will constructively interfere only for given values of θ, the inclination angle of the incoming wave to the crystal plane in question. The phase factor which we can write as $\exp(\mathrm{i}\mathbf{q} \cdot \mathbf{R})$ must then be 1 so all pairs of lattice points with the distance vector $\mathbf{R}$ or an integer multiple of this vector between them will interfere constructively. Thus $\mathbf{q}$ must for constructive interference to happen equal the reciprocal lattice vector,

$$\mathbf{q} = \mathbf{G}, \tag{1.11}$$

which is called *Laues condition*. $\mathbf{G}$ is defined by [7]

$$\mathbf{G}_{hkl} = 2\pi \widehat{\mathbf{n}}_{hkl} / d_{hkl}. \tag{1.12}$$

This is a vector which is normal to the crystal plane designated by the numbers hkl, and since $\mathbf{R}$ must be an integer multiple of the dimensions in the unit cell, we have got the fundamental results for diffraction under the limiting conditions of a perfect crystal. This will help us deduce Bragg's law which can be deduced by a geometrical consideration

under the requirement that path differences between scatterers should be an integer multiple of wavelengths. We have $G = 2\pi n/d_{hkl} = q$ giving us

$$2\pi sin(2\theta/2) = n\lambda \tag{1.13}$$

which evidently is *Bragg's law*.

To sum up the results from this derivation, consider Ewald's sphere which provides a more tangible realization of facts. This construction which is also called the reflection sphere provides a graphical way to render the reciprocal lattice to scale with the radiation used, but also to find which reflections of different Miller indices can be seen with a crystal in a certain orientation.

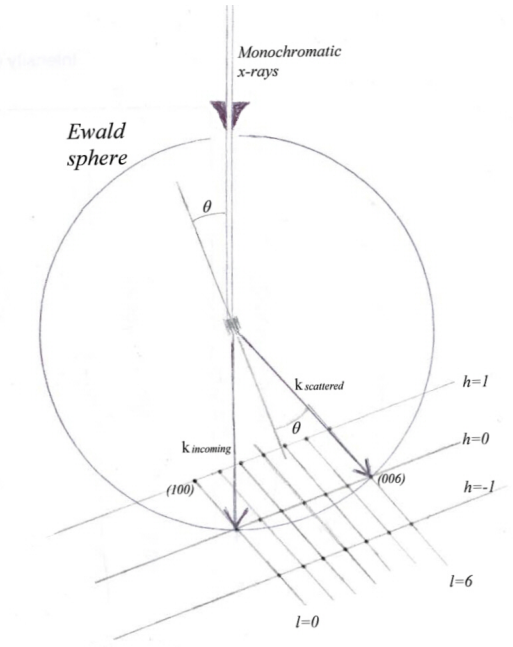

Figure 1.3: Schematics of a Ewald sphere with its reciprocal lattice for a layered single crystal clay particle. The projection of the sphere is seen in the k=0 plane of the reciprocal lattice. A portrayal of a clay particle is situated at the scattering centre for illustration of the scattering geometry and the (geometrical) link to the reciprocal lattice.

The origin for the reciprocal lattice in figure 1.2.2 is where the $\mathbf{k}_{incoming}$ is ending at the bottom of the sphere. The radius of the sphere is $|\mathbf{k}_{incoming}| = \frac{2\pi}{\lambda}$. The requirement that $\mathbf{q} = \mathbf{G}$,means that $\mathbf{k}_{scattered}$ should end on a node of the reciprocal lattice. That is because the origin of the reciprocal lattice is also the starting point of the scattering

vector. The nodes in the figure are Miller indices for the crystal and we can by the construction of the Ewald sphere and the reciprocal lattice find which reflections is possible for a given wavelength and orientation of the crystal.

We have found the unit cell structure factor for the general case, and we consider now the reflections $(00l)$ from a monoclinic 2:1 clay mineral. There is then a symmetry in the z-direction, perpendicular to the $a \times b$ base of the monoclinic cell. The symmetry allows cancellation of the imaginary part of the complex phase.

$$F(00l) = \sum_n f_n \exp(\boldsymbol{q} \cdot \boldsymbol{R}) = \sum_n f_n \cos(4\pi * z_n \sin\theta/\lambda). \qquad (1.14)$$

The first function F$(00l)$ shown in (1.14) is discrete, but the last equality introduces, by invoking the value for the scattering vector, its continous counterpart which is the *layer scattering factor*[2], and will be referred to as G(θ). This will constiute a principal factor in determining peak positions, relative intensities between them and other peak characteristica of the intensity spectrum. The intensity is proportional to the layer scattering factor squared since I $= |\boldsymbol{E}|^2$.

The formula expressing the polarization of the wave has two terms. The first one which equals 1 is when the polarization of the wave is in a certain plane, and the scattered radiation is in a perpendicular plane to this. When it happens in the same plane we will get a term $\cos^2(\theta)$. Not using a coherent source, we get equal contribution from both factors and we get therefore

$$\mathrm{P}(\theta) = \frac{1 + \cos^2(\theta)}{2}. \qquad (1.15)$$

When the beam hits the sample it will be presented to a volume of the increment of the crystal exposed[2], and only a certain fraction of the crystals will be aligned for diffraction. These two factors are multiplied and merged with the polarisation factor to have the Lorentz-polarisation factor:

$$\mathrm{L_p} = \frac{2\mathrm{P}(\theta)}{\sin(2\theta)\sin(\theta)}. \qquad (1.16)$$

for perfectly random powders. The factor (L$_\mathrm{p}$) is a macroscopic geometrical factor and is proportional to the intensity.

The effect of the limited amount of layers will create ripples at other values than the angles for Bragg peaks. This can be considered equivalent to the situation of a diffraction grating where the distance between the slits are the same as the d-spacing($d(001)$) and the number of slits, $(N-1)$ will be the number of layers in the crystallite. By

Fourier-transform[8] of such a diffraction grating one gets the interference function $\Gamma(\theta)$,

$$\Gamma(\theta) = \frac{\sin^2(2\pi N \sin(\theta) d(00l)/\lambda)}{\sin^2(2\pi \sin(\theta) d(00l)/\lambda)}. \tag{1.17}$$

At central maxima the intensity scales as N^2, and the amount of ripples inbetween is $(N-2)$.But since we are almost always dealing with a macroscopic sample there is no reason to believe that there will not be a distribution of different N in the diffraction volume so a distribution of different particle sizes is called for. Probabilities of finding a particle with N layers is p_n and we get the following normalized (the summation of p_n equals 1) interference function [2]:

$$\Gamma(\theta) = \sum_{N=n_1}^{N=n_2} p_n \frac{\sin^2(2\pi N \sin(\theta) d(00l)/\lambda)}{\sin^2(2\pi \sin(\theta) d(00l)/\lambda)}. \tag{1.18}$$

There are good reasons to believe that the number of layers in the different particles follow a Log-normal distribution[8, 9]. A profile resulting only from different particle sizes has been calculated and can be seen in figure 1.2.2. In the figure it is seen that the distribution leads to a smoothing of the profile, but that the minima in the profile don't disappear completely. Since profiles showing such minima are not (or very rarely) observed in reality it is clear that the model here presented is too far from real conditions for the most clay particles.

The final intensity is thus

$$\mathrm{I}(\theta) \propto \mathrm{L_p}(\theta)\mathrm{G}(\theta)\Gamma(\theta). \tag{1.19}$$

For many experiments on a single clay mineral and different setups without large disturbances or biases the factors contributing to intensity are in fact mostly sufficient for qualitative assessments and to some degree quantitative assessments of the diffraction profiles. In fact these expressions posess the generality to take a first step towards describing detailed characteristics of the swelling and particularly giving us general ideas to the structure and amount of water in the interlayer. By fitting the layer structure factor, you can substantiate or develop a model for distribution of particles in the interlayer[3]. Furthermore a detailed description of dynamics and mixed intercalation states is possible [10, 11, 12, 14] the lower range of possible angles in a Wide-Angle X-Ray Scattering(WAXS) experiment.

[8] A Fourier-transform is in fact what has been done for all the steps , first for one atom, then the unit cell, and now to find the intensity of the full crystallite or clay particle.

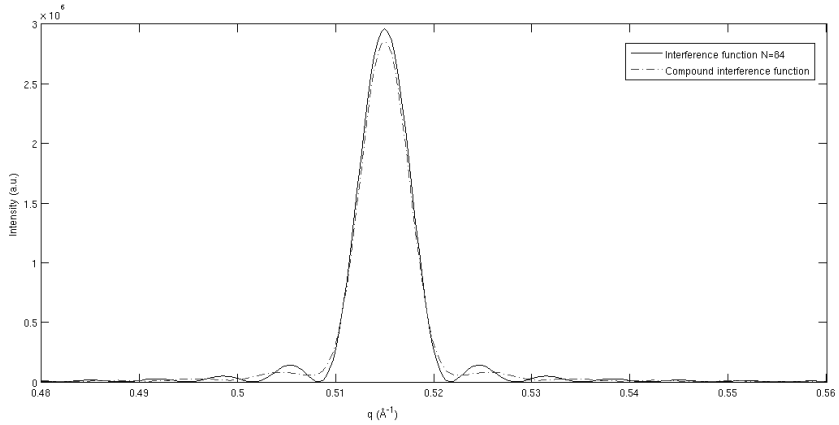

Figure 1.4: Interferencefunction from a number of (normalized to the other profile) particles with 84 layers and from a distribution of number of layers in particles with a mean of 84 and a standard deviation of circa 30. 500 samples were drawn randomly from a log-normal distribution from which the complete profile was calculated.

1.2.3 Intercalation in Clay Minerals

For clays which do not have negative layer charge the surfaces will easily be broken asunder, and have a well-defined cleavage[35] [9]. Although there is controversy as to relative importances of different causes for swelling in clay minerals[5], an outline for the proposed most important causes follows. Cations are counterions for the negatively charged surface of clay minerals and causes the two layers to bind toghether. So the attraction from the layers from the top layer to the cation as well as the bottom layer, will create an equilibrium position because the double layers created on each surface oppose eachother. There are also types of bonds other than the ionic bonds and the electrostatic forces to consider. Most notably is that of hydration; this is for most clay minerals the main contribution to the swelling [5]. Hydration will lower the free energy of the total system when there is relative abundancy of water molecules present. The water molecules or alternatively organic molecules or polar molecules will diffuse into the interlayer space, making the entropy larger, and naturally increasing the basal spacing as the layers of water are fitted into the interlayer structure.

The hydration forces includes ion-dipole, co-ordination bonding, hydrogen bonding and van der Waals bonding [35] to mention the most

[9] Well-defined clevage mean that an elementary crystal face (with low Miller indices) defines a large part or all of the surface of the macroscopic particle

substantial ones. The ion-dipole and co-ordination bonding will produce complexes with the cation. Such complexes can be formed as either outer-sphere or inner-sphere, according to whether it is placed in the interlayer or in hexagonal cavities in the tetrahedral sheet.

1.2.4 Peak Characteristica and fitting with Pseudo-Voigt function

Peaks that are composed only of one defined basal spacing will, if we have a rather well structured interlayer of molecules, be quite sharp for Fluorohectorite, as these will typically have around 100 layers[10].

The signal to reach the detector will presumably have the intensity described by equation (1.19). This signal as a function of q is known to resemble a Lorentzian to a fair approximation[3]. This is caused by equation (1.18) which for the different amount of layers present in different particles do away with ripples from one $(00l)$-reflection to the next. We therefore choose to model the intensity spectrum to a Lorentzian function. But peak broadening can also be due to experimental setup, and certainly by instrumental resolution or noise. These effects are usually Gaussian distributed. Since these effects of the different variables summarize to give the measured signal, a convolution is called for to find the distribution for the measured signal. The result of the convolution of a Gaussian and a Lorentzian is called the Voigt function. But the problem with this function is that there does not exist an analytical solution .The applied function is therefore the PseudoVoigtian function:

$$\mathrm{pV}(q) = \eta \mathrm{L}(q, \omega_{\mathrm{L}}) + (1-\eta) G(q, \omega_{\mathrm{G}}) \tag{1.20}$$

where $\mathrm{L}(q)$ and $\mathrm{G}(q)$ are the Lorentzian and Gaussian contributions, and η is called the shape factor. η is between 0 and 1 and determines the shape of the curve. ω_{G} and ω_{L} are linewidths attributable to each of the two functions' contribution. They are related to ω and η in the following more complete formula

$$\mathrm{pV}(q, q_c, \omega) = A\Big[\eta \frac{2}{\pi} \frac{\omega}{4(q-qc)^2+\omega^2} + (1-\eta)\frac{\sqrt{4\ln(2)}}{\sqrt{\pi}\omega} \exp(\frac{-4\ln(2)}{\omega^2}(q-q_c)^2\Big] \tag{1.21}$$

By fitting these equations there exist arithmetic relations that give the value of ω_G and ω_L. For details refer [36, 37].

[10] The distribution is probably quite broad, and can not be measured as (it) is without elaborate sample preparation.

1.2.5 Random intercalation states - Hendricks-Teller formulation

If there is random interstratification, meaning that there is different basal spacings between the layers in a particle, there will generally not be the sharp peaks of particles with basically only one basal spacing between layers. Hendricks and Teller have dealt with different situations of intercalation[29] and found formulas for diffraction profiles for different situations of random intercalation in layered lattices. If there is order over a long range of layers we can expect to get contributions of the pure peaks for the two basal spacings. For if there is a long range order, the number of layers N (see equation (1.18)) of one basal spacing will be high, and will produce a sharp peak. If however this order does not exist, i.e. if the stacking inbetween one interlayer is independent of the next interlayer,the diffracted profile will be broadened even in the case of very few (e.g. 2, stacking two layers, A and B, randomly on top of eachother) discrete spacings existing in the stack when these does not have too large relative difference in spacings between them. Hendricks and Teller's[29] most basic formula was calculated on the following assumptions:

- Only two discrete spacings exists between layers of equal scattering power
- The fractions of each spacing is the same
- There is no (or a negligible amount of) interlayer material
- There is no correlation from one layer to the next, i.e. completely random stacking

The idealizations to receive the formulas were that the X-rays were diffracted from crystals of infinitely many layers, from a non-divergent, perfectly monochromatic beam. The formula they found depends on the phases for two different spacings (either A or B), ϕ_A or ϕ_B and their mean $\bar{\phi}$

$$I_{av.} = V^2\Big(\frac{1-(\cos\frac{1}{2}(\phi_A-\phi_B))^2}{1-2\cos\bar{\phi}\cos\frac{1}{2}(\phi_A-\phi_B)+(\cos\frac{1}{2}(\phi_A-\phi_B))^2}\Big) \qquad (1.22)$$

and V^2 is the layer scattering factor squared. Hendricks and Teller shows that under these conditions a peak will be quite sharp and intermediate to the two different spacings. Since the system these calculations was done on was a hydrated montmorillonite, the results, both theoretically, and to some degree in experiments is very likely to carry

over to fluorohectorite. Hendricks-Teller (HT) states have previously been indicated to be present in NaFH in reports by Hølto, Alme and Løvoll[11, 10, 34].

1.3 Hydration phase transitions

The causes of water intercalation in clays have previously been discussed. Now the free energy of the water hydration in the interlayer space will be briefly discussed. The Gibbs free energy for hydration termed G_{hydr} is by definition

$$G_{hydr} = H_{hydr} - TS_{hydr} \tag{1.23}$$

where S is the system's entropy, T its temperature and H is the enthalpy. The change in G_{hydr} while keeping T constant can be expressed([31, 13] as in the following form:

$$G = [V_{hydration}(i) - RT \cdot \ln(\frac{P_{vap}}{P_{vap}^{sat}})]n(i) \tag{1.24}$$

where $V_{hydration}$ represents the hydration energy associated with one water molecule, R is the gas constant, the relation between the vapor pressure of water P_{vap} to the saturated vapor pressure defines the relative humidity(RH) in air. The amount of water molecules in the interlayer sheet is $n(i)$ and i signifies the water intercalation state. The term $RT\ln(\frac{P_{vap}}{P_{vap}^{sat}})$ is called the external field[31]. The hydration energy and amount of water molecules intercalated depend strongly on the amount and sort of cations intercalated (as the whole clay unit structure does), but these contributions to the hydration will implicitly lie in $V_{hydration}$ and $n(i)$. In a smectite it is said that between zero to three water layers can be intercalated into the interlayer space. This can sometimes be a loose determination and will most likely for a given clay intercalating particle not correspond accurately to structuring and mechanisms for hydration in the interlayer space. However, in Sodium-Vermiculite, Sodium-Montmorillonite and Sodium-Fluorohectorite there are equilibrium states with d-spacings(001) from zero to two water layers(2WL), i.e. the d-spacing are linearly dependent on the amount of water layers, and the difference between one water layer state and the next is approximately the size for a water molecule(which, when bonded,is $\approx$ 2.3 Å) [35, 31, 3]. Vermiculite have a bigger negative layer charge than fluorohectorite, and montmorillonite is a dioctahedral clay; otherwise the clays are very similar. Equation (1.24) testifies how the relative humidity will influence the free energy of hydration. As just discussed

the different water intercalations(1WL etc.), represent different phases since they are in equilibrium. A phase transition between 1WL and 2WL, to a first crude approximation, ensues when the difference between hydration energies for different hydration states are relatively smaller than the contribution from the external field. Although the external field pushes one direction, a barrier must be overcome to either fit an extra layer in, or loose a water layer. If the situation was indeed that of either a 1WL state or a 2WL and nothing else this situation would fit perfectly into the formalism of the *Landau free-energy model*[11][7]. The phase transition in clay swelling is known to be a first order transition[31], which for the case in question means that there exists a discontinuity in the first derivative of the free energy with respect to P_{vap}.

[11] This theory links the free energy of a system to different order-disorders of states in the system.

Chapter 2

Experimental section

In describing the different experiments four crucial aspects of it will be discussed in order. This is done for each of the three experiments carried out.

- Experiment design
- Experimental equipment
- Control, data collection and uncertainty
- Method of Analysis

2.1 Hydration phase transition

2.1.1 Experiment design

The goal of the setup which was constructed was to hydrate clay powder at a given constant temperature, and measure how d-spacings depended on humidity.

To control temperature of the sample cell a quite elaborate, but flexible, design had been chosen. A temperature controller unit operated a resistance heater element with the negative feedback coming from a temperature sensor attached to the sample cell. The temperature controller had a built-in PID-regulator[1] which could hold it at a constant temperature by providing the correct heating effect at a given time. But because the sample holder also needed to be held below or in proximity of room-temperatures some cooling of the sample cell was

[1] A PID-regulator regulating temperature by a heater will calculate the difference signal from the reference signal to the measurement signal. It will deliver a gain to the heater proportional (P) to the difference signal, an integral(I) of it or a derivative(D) of the difference signal.

needed. For this purpose a Peltier-element with water cooling of its hot side was installed.Thus by setting the right effect to the Peltier-element, the temperature controller unit would control the temperature of the sample cell to the correct set-temperature.

Controlling humidy, and keeping it constant was the crucial thing for this experiment. For this purpose unequal amounts of dry and moist air was mixed to give the relative humidity desired.The mixed air was then delievered to the sample cell. Inside the sample cell the powder sample had been packed into a cylinder-shaped hole in a copper holder attached to the sample cell. Almost being insulated from the environment outside of it the sample cell can achieve a wide range of temperatures and nearly the whole range of relative humidity.

2.1.2 Experimental equipment

The sample cell

The sample cell is a two part assembly with a copper base and a cover of aluminum. On the top of the cover there is a hole to insert the humidity probe. Its base has fitted a Peltier-element to it, furthermore it has two hose fittings for inlet and outlet air, hole for a sensor, and a cavity with copper foam connected with the inlet. The copper foam makes sure the incoming air has the same temperature as the sample cell. A picture of the sample cell set in place for measuring is shown in figure 2.1.

Constant humidity solutions and peristaltic pumps

For control of the relative humidity a constant mixing ratio between two volumes of fixed humidities was achieved by using two peristaltic pumps with variable speed. The peristaltic pumps' output was joined and provided the fixed input air for the sample cell. The wet humidity solution was saturated salt solution of *Potassium Sulfate* (or K_2SO_4) which provide about 97% RH[19] at 25°C above its surface.The dry air came from the air which had been in thorough contact silica gel, a desiccating agent which can give humidities down to about 1 % RH for standard setups. The two peristaltic pumps was of the brand *Heidolph*, model PD5001. This delievered, with the utilized silicon hose dimensions, from about 30 ml/minute with the minimum effect to about 400 ml/minute[2][15].

[2]This was not measured, but taken from reference[15].

Temperature control unit

The Lakeshore 321 was the regulator unit which controlled the temperature. It controlled against a reference signal of a thermocouple type K sensor inserted into a hole filled with thermal paste. The heater element had a maximum effect of approximately 20 W, but was not used to more than 20% of this during the experiments. The regulator, according to specifications, and evidenced by performance, was able to regulate within 0.1 ° C accuracy.

The thermocouple input signal to the Lakeshore unit was calibrated to give an accuracy of at most 0.2 ° C. The calibration was done against boiling water and ice water references.

Humidity measurement

The humidity probing instrument used was HMI38. The humidity probe was HMP37E and selected specifications of this meausuring system are given in table (2.1)[16]. The Humicap sensor was a capacitance

Table 2.1: Specifications for the humidity measurement instrument

Humidity sensor	Humicap H-sensor
Temperature sensor	Pt 100
Operating temperature	$-40 - 130°$C
Measurement range	0-100 %RH
Resolution	0.1 %RH
Accuracy	2 %RH with field calibration
Response time	15 seconds

between two electrodes, and this capacitance changed according to different humidities. The Pt 100 temperature sensor is a Platinum sensor element on which the resistance through it is measured.

Calibration for the humidity sensor was done using two saturated salt solutions of LiCl and Nacl for dry and wet calibration respectively. The values, which was taken from tabulated values by Greenspan[19], was for the LiCl-solution 11.3 %RH and for NaCl 75.3 %RH. The calibration action itself was to turn a screw until the correct humidity on the panel was reached. This could be done to an accuracy within 0.1 %RH. The temperature calibration of the probe was done against the thermocouple and did not need adjusting.

When calibrating there were two general and decisive concerns to handle. The first one was materialistic, dealing with the calibration

salt [3], its cleanness, making sure that the seal was perfect, etc. The second concern was with the temperature and was more challenging. It was crucial to prevent large temperature gradients between the probe and the solution as this would affect the humidity measured. For this reason primarily it was essential to have the humidity probe near the actual surface. For the setup used it was not possible to measure this gradient, but only give a general idea of its importance. As reported previously[10], it is important to hold the environment as well controlled as is practically manageable. Equilibrium for the relative humidity for the different salt solutions was reached after 24 hours and for some calibrations somewhat longer.

The finished setup with the probe inserted is seen in figure 2.1. The humidity probe was inserted on the top of the cover. It was fixed so that the sensors were situated a couple of centimeters above the sample and the sample chamber was then sealed off from the outside.

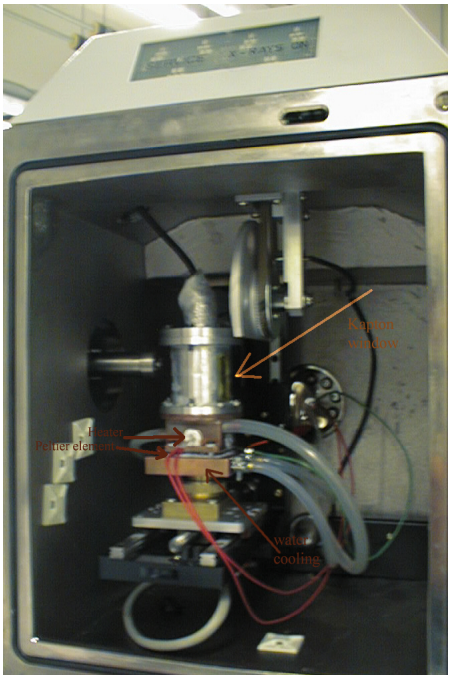

Figure 2.1: The X-ray beam comes in from the tube to the left in the picture entering a Kapton window, scatters from the sample and leaves through the X-ray kapton window indicated travelling to the Nanostar detector further right, not seen in this picture.

[3]Some believe that it is not merely enough to have a saturated solution, but that there should be a sludge, with just a small layer of the saturated phase at the top of the sludge(/solution).

2.1.3 Control, data collection and uncertainty

Controlling humidity

During the preliminary experiment it turned out that although the flux of both wet and dry air was held constant it was difficult to achieve a stable humidity in the sample chamber within an hour. Therefore the improvement was made that an extra reservoir of humid air in the form of another potassium sulfate solution was put in series with that of the reservoir leading to the sample cell. This was also done for the silica gel side, and this improved the performance of the regulating system considerably. Regulation was done via knobs on each of the pumps. Increments of 1 % was the goal but not always achieved. If overshooting the increments by turning the knob slightly more than wished for, data points would be missed as we were studying a phase transition which was an irreversible process. But sometimes, because of time constraints, there was not the option of going less than 1 % increments and therefore, a cautious continous regulation of the knob was done to get the correct increment. This of course led to small inadvertent overshoots. Because of the porous nature of the copper foam, the hydrating properties of the powder, temperature gradients effect and of course time lags of the instruments there were considerable time lags of different orders the humidity regulating system. One interfering effect which was appreciated only after some time into the experiment was the warming of room temperature caused by the presence of humans being a temperature source. This made the salt solution introduce more water vapor to the humidity cell by an amount of $\approx 1\%$ RH.

Temperature gradients and normalized humidity

The sample was held at 25°C but the humidity probe had a temperature of about 0.9°C above this. This was caused by the larger temperature inside the X-ray chamber which was at $\approx 29\circ$C. The room temperature was 24-25°C. The transformation of relative humidity has to take two things into account:

1. The change in vapor pressures at different temperatures
2. The change in saturation vapor pressure at different temperatures

To get the transformation formula we use the ideal gas law, the definiton of relative humidity and a formula for finding saturation vapor pressure. Using the ideal gas law for the vapor pressures at two different temperatures, assuming same displacement and molar amounts , we divide the partial vapor pressures by eachoter. Using variables p_{sample},

p_{probe}, T_{sample} and T_{probe} we get that $p_{sample} = p_{probe}\frac{T_{sample}}{T_{probe}}$. Taking into account that the vapor saturation pressure depends in a nearly exponentailly way on temperature, this makes the largest difference for the relative humidity at all but the low humidities. So, only by invoking the definition for the relative humidity,the relative humidity for the sample is

$$RH_{sample} = RH_{probe}\frac{p_{probe}^{saturation}}{p_{sample}^{saturation}}\,\frac{T_{sample}}{T_{probe}}. \tag{2.1}$$

The formula used to calculate the saturation vapor pressure was formulated by Wagner and Prußen[32].

Uncertainty in d-spacing

In this experiment it is practical to consider two different uncertainties relating to d-spacings. The first quantity is the absolute and actually measured d-spacing. The associated uncertainty comes primarily from error in the calibration of the sample to detector distance but also from factors such as uncertainty in the wavelength, sample broadening, detector resolution and a non-collimated beam. The calibration of the sample to detector distance was done using the reference sample Silver Behenate with a large d-spacing, giving multiple Bragg diffraction rings which rendered it possible to have a very precisely defined beam center position (which was important when integrating 2D-data to diffraction profiles), but more importantly, to find the correct sample to detector distance. The calibration procedure gave a sample to detector distance of $259.3 \pm 1.5\,\text{mm}$, which gives an uncertainty in the d-spacing of about 0.03 . Taking into account broadening effects; the most substantial factor to this being the extension of the sample in the beam direction which was $1.5\,\text{mm}$ a more conservative estimate is made of 0.05 as the uncertainty in d-spacing.

The other type of uncertainty is the relative d-spacing, i.e. the uncertainty from one measurement to the other. The most important contributor to this uncertainty apart from detector resolution, was the limited counting statistics for each measurement point. The measuring time for one run or data point was 30 minutes and with the existence of a relatively sharp peak this amounted to about 16000 counts in the diffraction profile. This was without the background noise from the detector and air scattering subtracted. However these factors were small in comparison to the signal. The uncertainty in relative d-spacing in a conservative estimate is $0.02\,\text{Å}$ but is thought to be significantly higher for the more disordered hydration states. This implies that the

uncertainty in relative d-spacing in this experiment is larger in the range of the hysteresis curve.

Detector characteristics

The detector used was a multiwire grid "Histar" (from BRUKERaxs) with 1024x1024 pixels. It uses pressurized xenon gas at 5 bars as the ionizing agent. The spatial resolution is 220 μm, which is just over 2 pixels in length. The detector has a level of dark current noise of ≈ 7 counts per second per frame.
In table (2.2) parameters for the phase transition experiment are gathered.

Table 2.2: Phase transition experimental parameters

Sample temperature	25°C
Measuring range	5-92 %RH
Absolute uncertainty in d-spacing	0.05
Relative uncertainty d-spacing	0.03
Humidity stability	0.3 %RH
Accuracy of humidity measurement	3 %RH
Stability of RH for one humidity measurements	0.3 %RH

2.1.4 Method of analysis

The diffraction profile was fitted with two different peaks of the PseudoVoigt function with different Lorentzian and Gaussian widths. The center of the most dominant peak was selected to find the d-spacing using a simple equation(1.12). Where none of the peaks was dominating the total diffraction profile a mean depending on the amplitude on the position of the different peaks was calculated. The diffraction patterns from the detector had to be integrated over the azimuthal angle from the"SAXS" software to receive the diffraction profile depending on the angle two theta which was transformed to the value for the scattering vector.

2.2 Mixed water intercalation states in NaFH

2.2.1 Experiment design

The experiment was done at Pohang accelerator laboratory(PAL), a synchrotron in Pohang, Korea at beamline 5C2 which belongs to Gwangju Institute of Science and Technology(GIST). Setting up a humidity gradient along a thin quartz capillary with NaFH-powder different intercalation states of the sample could be studied. By manipulating the beam size different resolutions for probing the sample both in parallel to and across the gradient was possible. For the smallest scales this would not be practically feasible with standard equipment on a regular laboratory source.

The sample powder inside a quartz capillary was situated on a copper block which regulated the temperature for the sample. Three pairs of slits along the beam path inside the hutch(the experimental chamber) defined the beam dimensions from the already coarsely focused beam from the focusing device of X-ray mirrors and bent Silisium crystal monochromators. The humidity gradient was established by utilizing silica gel and a saturated potassium sulfate solution.

2.2.2 Experimental equipment

The storage ring operated with a beam energy of 2.5 GeV, and the bending magnets has a field of 1.3 Tesla [17]. This gives a critical wavelength of 2.3 . For all the measurements harder X-rays were chosen with a wavelength λ =1.244 .

Detector

The detector was a CCD-camera of diameter 1.3 cm, with an X-ray phosphor screen coupled fiberoptically in a 1:1 ratio to the CCD-detector. The pixel frame was 1024x1024 and pixel size was 13x13 μm. It claims to have resolution of 38 lp/mm[24] which makes the effective resolution be 2 pixels. Due to its small diameter it could in the setup be situated only to see about one third of the Debye Scherrer ring. The beam stop used to protect the detector was a rectangularly shaped tantalum piece.

Sample and humidity gradient

A quartz capillary with diameter of 1 mm, and wall width of 10 μm, was filled with NaFH-powder. It was cut at both ends, and put on top of the copper cell. Near the copper cell's two ends there was a hole

on to which via hose fittings a humidity reservoir could be fitted. A cap together with silicon glue sealed off the capillary from the outside air. For most measurements the sample was held at 15±0.2°C. The high relative humidity was provided by potassium sulfate salt solution, together with wetted blotting paper through the hose connected to the wet side. On the dry side spherical single silica gel grains was put in two small hoses directly connected to the cavity for the one side of the capillary. The setup can be seen in figure 2.2.2.

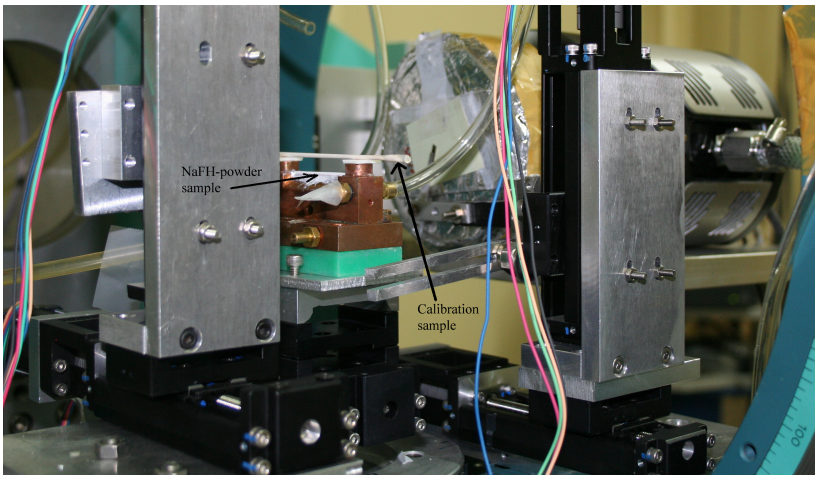

Figure 2.2: The sample setup in an initial phase.The rectangular plate to the left of the copper cell was the holder for a y-drive motor which supported manually assembled slits. The calibration sample of Silver Behenate is shown above the sample itself. The detector is shielded while measuring the beam position by use of a burn papir.

2.2.3 Uncertainty and data collection

The biggest source of errors for the measured values themselves was also this time the calibration, and sample broadening effects. Since the sample was so close to the detector, at only $\approx 10\,\mathrm{cm}$, the extent of the sample was contributing to the width and, to a much less extent, to the shape of the profile. Calibration was done with Silver Behenate powder inside a 2 mm capillary.

2.2.4 Method of analysis

Captures or frames collected from the detector were stored in a format(with the suffix .imm) relatively specific to an interpreted program-

ming language called *Yorick*[4]. The detector had a quite large dark current background signal. This signal together with the no-sample scattering characteristics of the direct beam was recorded in background scans. Because the detector could be saturated at some pixels measuring times for one frame was typically only 10 seconds, necessitating taking many frames to get one diffraction pattern for analysis. The addition of multiple frames and subtraction of background was done by utilizing special scripts. Conversion of the resulting image files to tif-files was performed to do the raw analysis in the program *fit2D*.

2.3 Fluorohectorite wide angle diffraction profile

2.3.1 Experiment design

A sample of Nickel-Fluorohectorite was put in a distance to the detector to see at least the d(006) peak of the diffraction pattern. A special sample cell and a customized extension unit was designed by the author and made by the NTNU machine shop. This sample-cell provided the opportunity to manipulate humidities to almost the full range of relative humidities and temperatures for the sample from well below freezing to temperatures above 100 degrees Celsius. In the experiment carried out a bath of a saturated salt solution(NaCl) was placed inside the sample cell to keep the RH constant while changing the temperature.

2.3.2 Experimental equipment

A water bath in quite good thermal contact (via Kapton Tape) with the copper floor of the sample cell was made of silicon walls. The dimensions of it were maximized to achieve equilibrium with the powder sample at quickly at different temperatures. That the dimensions were sufficient for this purpose was established by reviewing [18].The sample cell was designed by the author, made of Teflon and copper to withstand a large range of temperatures. An extension unit and sample cell holder was also designed and made at the workshop. A flat Kapton-encapsulated heater element was attached on the bottom of the sample cell, and connected to the Lakeshore temperature controller unit. Because of big background scattering from air lead shields were put in place to stop it. A lead screen acting as an anticscatter pinhole is seen put in place inside the sample cell in figure 2.3(b).

[4]Yorick is written in the C language, and has extensive graphical capabilities and efficient array manipulation [33].

Sample

The sample was from a batch which was cation exchanged by Tommy Aalerud, a former master student, purchased from Corning Inc. in the form of pellets of LiFH. The NiFH was packed in a 1 mm capillary, and the capillary was cut across to make cylinders of length less than 2 mm which was fixed/supported inside a copper sample holder. In figure 2.3(b) the sample is shown sitting inside the sample cell before an X-ray transparent window sealed the sample cell off from the environment.

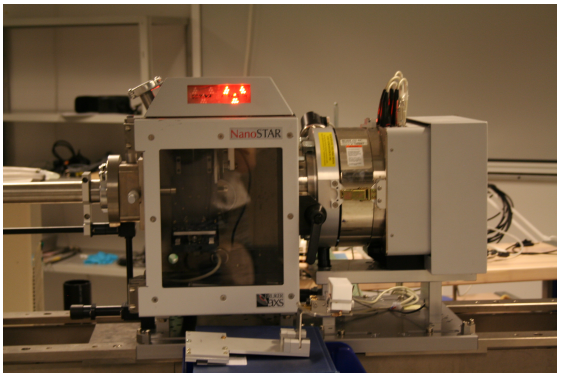

(a) Sample cell in front of X-ray chamber

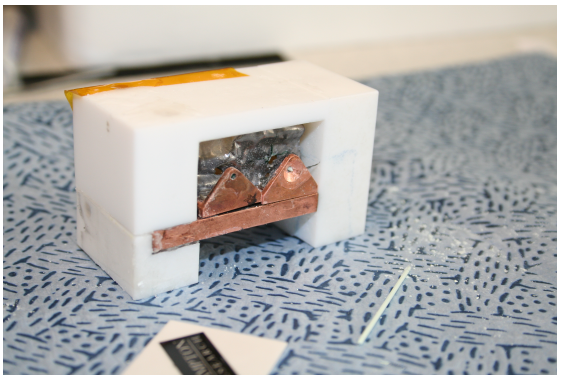

(b) Sample in place

Figure 2.3: The sample and its extender before mounted on the sample stage in X-ray chamber

Detector

The previously mentioned HiStar detector at NTNU was utilized for the measurements. Calibration procedures had to be done for the new

detector to sample distance. This was done by installing a radioactive isotope, Fe-55, in the sample position, recording a so-called flood-field to normalize the intensity across the detector. The second, and very important calibration, was the spatial correction which was done to prevent that the near flat(it is slightly curved) detector with its x-y grid would image the diffracted intensity at wrong points. The procedure for this was again to set the Fe-55 in the sample position, and put a brass plate with an array of holes in front of it to let it record a pattern from which the needed spatial corrections would be calculated.

Heaters and salt-solution

To heat and control the sample cell's temperature the same principial setup was used as in the phase transition experiment. A flat resistive heating element was placed directly under the bottom of the copper base of the sample cell, and a copper plate below this element was screwed fast to the base of the sample cell. Below this a Peltier element was placed, and below this a cooling element for the Peltier element connected with circulating water to a water bath. The salt solution was selected for its extraordinary stabillity to maintain the same humidity at different temperatures as well, of course, with its availability. NaCl has not more than 1.5 % difference in RH over the temperature range 0-75°C[19]. The only thing left desired for the solution was that it would have a slightly smaller relative humidity bringing it presumably closer to a phase transition between 1 and 2 water layers which for NaFH has been shown to be about 60 %RH.

2.3.3 Data collection and uncertainty

Even from very thin samples of 0.3 mm broadening was at FWHM one degree or more at diffraction angles of about 30 degrees. A shift of profiles of maximum one degree could also be detected due to sample broadening. For data collection to be reliable a good calibration with the Fe-55 source had to be made. This calibration was the basis for unwarping the frames which was visibly distorted. The calibration gave satisfactory results. In other respects the data collection was as in the phase transition experiment.

2.3.4 Method of analysis

The frames were integrated to give one-dimensional profiles on which the analysis were done in the software Origin.

Chapter 3

Results and discussion

3.1 Phase transition

Two scans in the analysing software "SAXS"(BRUKER Axs) are shown in figure 3.1. For the mixed intercalation state showing two maxima at degrees roughly corresponding to 1WL and 2WL it is not easy to transform this data to d-spacings in a completely non-ambigous way. It was chosen to take a weighted mean between the two maximas, but this method has big uncertainties owing to randomness in the chosen weighted parameters.

The results of the phase transition experiment on NaFH at 25°C are seen in figure 3.1. Clearly seen, though lacking some resolution in the curve of decreasing humidity, is a hysteresis. This is as expected since a phase transition occurs. Another experiment, with the same setup, and the same clay, was done by Alme([10]) at a temperature of 15°C. Central findings from both these two experiments are listed in table (3.1).

Table 3.1: Central parameters from two phase transition experiments on NaFH

	Alme	Kjelling
Temperature	15°C	25°C
Transition humidity	62 ± 2 %RH	62.5 ± 3 %RH
Hysteretic width	$11 - 14$ %RH	$9 - 13$ %RH
Humidity range	$4 - 92$ %RH	$4 - 92$ %RH

In the table it is seen that the two experiments differ almost only in the temperature they were performed at. The transition humidity is defined to be located in the middle of the hysteresis curve, and the

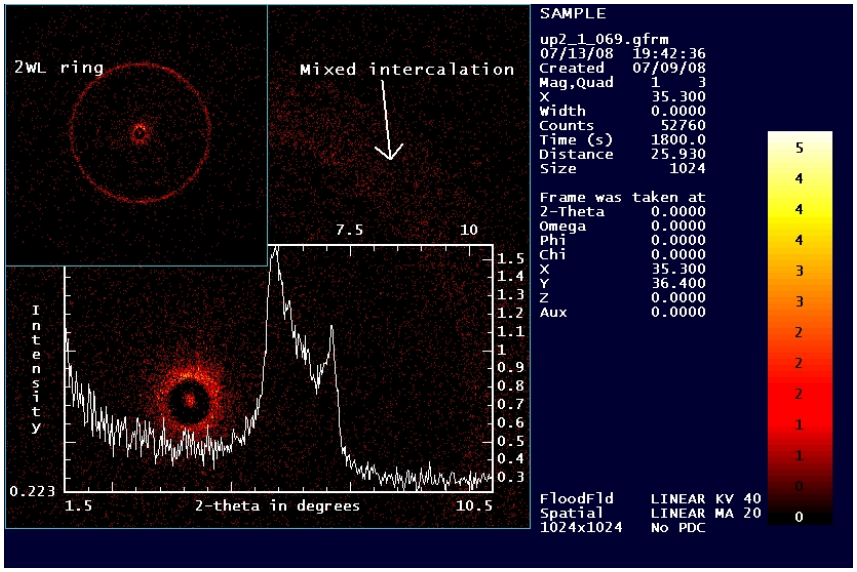

Figure 3.1: Two typical diffraction patterns from NaFH. The biggest part of the picture is a diffraction pattern magnified two times, offset somewhat, and integrated to get the one-dimensional intensity dependency on two-theta. In the upper left corner is a typical diffraction pattern from just one intercalation state. The relative humidity for the central part is about 69 %RH, and the inset frame is taken when RH was at $\approx 92\,\%$.

hysteretic width is the width between the curves. Since the exact way of how the hysteretic width was found, the difference in lower bounds will not be attempted to make any explanation of and it is obivous that the ranges fall well inside eachothers central values. The results of the phase transition experiments, (3.1) although the difference in temperature is small, gives indication that the Gibbs free energy of hydration is independent of temperature over an extended but finite range. A way to explain this physically is that while the external field of hydration pressure increases, meaning that there is bigger activity of the water molecules increasing their likelihood for bonding, the hydration bonds in the interlayer space gets weaker due to larger thermal energy of the molecules.

A preliminary attempt to find the limits of the range of a fairly constant intercalation state keeping relative humidity constant was attempted in the experiment on the wide angle diffraction profile of another fluorohectorite, Nickel-Fluorohectorite(NiFH). The experiment (WAXS) was however inconclusive in this regard.

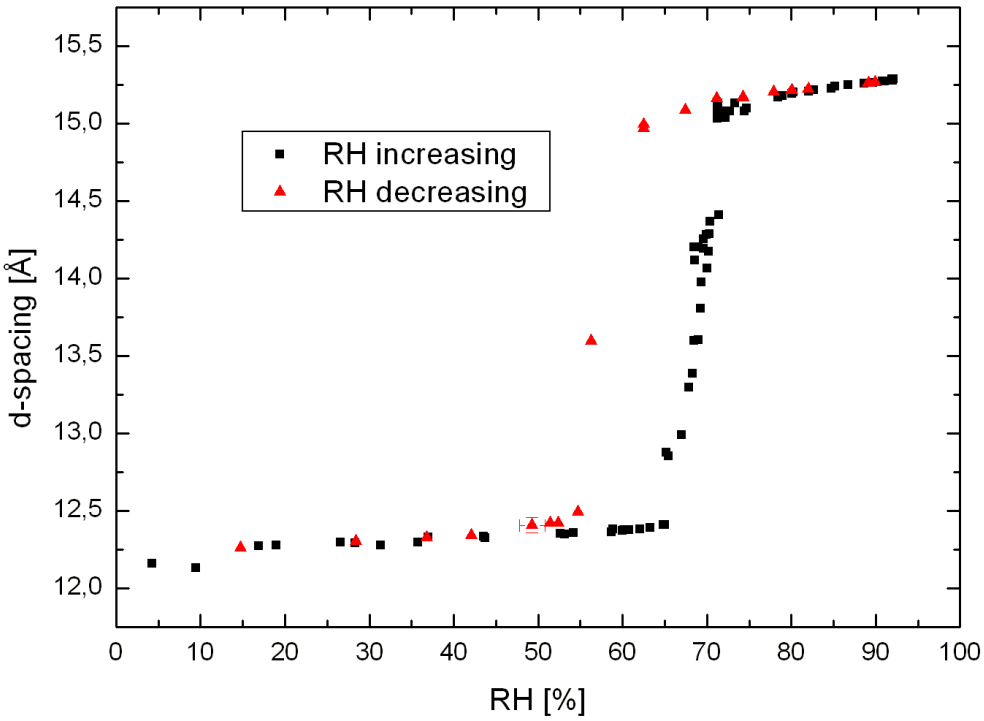

Figure 3.2: The phase transition in NaFH related to change in relative humidity. The error bars for all points except for in the transition region where the error is expected to be significant larger for the d-spacing is indicated at a point with RH of 49 %.

3.2 Mixed intercalation states in NaFH

As what was previously shown there exists a region, provided a certain humidity and constant temperature, in which NaFH have intercalation states which seem to be highly disordered having d-spacings of what looks like everything inbetween the 1WL and 2WL situation. But we know these profiles to resemble HT-states[11, 10] and a hope is to be able to resolve profiles to accurately attribute what kind of intercalation actually exists in the particles themselves. By probing along a hydration front at different length scales for the beam size the origin for the signatures for mixed intercalation was therefore investigated.

In figure 3.2 a collection of some different profiles along the capil-

lary is seen. The humid side of the capillary was at 0 mm. Particularly

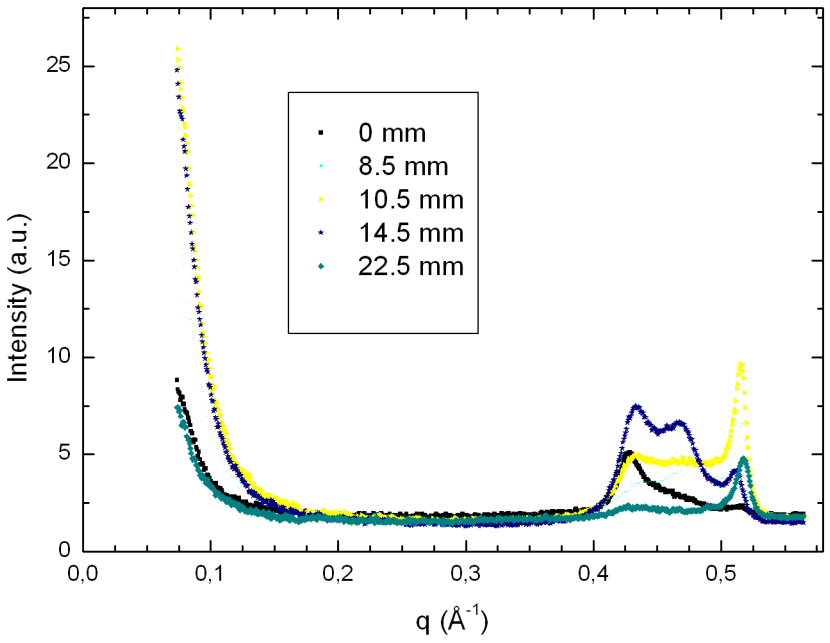

Figure 3.3: Some intercalation profiles along the capillary. A profile at 14.5 mm, with three peaks could have origin from random intercalation of 1WL and 2WL states.

one profile, at 14.5 mm, having three peaks is a profile needing some discussion since it is something not observed before in the similar experiments conducted before. A lack of diligence from the investigator's part could likely cause the wrong notions of what the diffraction profile is caused by. An obvious explanation is that a metastable state[1] with a d-spacing intermediate between a 1WL and a 2WL exists. Since such a diffraction profile has not been seen before this state would seem to appear under just the right circumstances. This however, the author thinks, is not a likely explanation since similar experiments, with and without a linear gradient, have not shown something resembling a peak at this position.

There are quite many number of ways of explaining this peak's ap-

[1] The state should figurally speaking really be hanging off a cliff (considering its potential energy), since it has never been observed before despite extensive experiments with equivalent designs[10, 34].

pearance even if we rule out that the peak represents a metastable state. The following discussion tries to point to most likely candidates for types of random intercalation to explain the ["suddenly appearanced"] peak. Figure 3.2 has a feature reminiscent of a pure random Hendricks-Teller state in that it has a peak, inbetween 1WL and 2WL positions. The shift to the left, towards lower q can on one hand be explained by the bigger contribution in this profile from the 2WL situation, but also on the other hand by the effect that the layer structure factor is substantially higher at lower q, hence a shift to smaller q is expected. But given that this explains the peak in the middle to be a HT-state, what about the two other peaks? There are two major different ways of explaining this special diffraction pattern. One way would be to say that a quasi-random ordering is prevalent in the crystals which give the diffraction signal. It means that there would exist a dependence on the state of one layer to the next one, but that this would be weak enough for randomness to exist to give a peak in the middle to give a HT-state.

The other way for explaining it would be to say that different crystallites have different intercalation states, which is not independent from crystallite to crystallite but depends on the surrounding environment of the clay particles consisting of micropores with absorbed water[39]. That is to say that different domains of water content contribute independently to the profile or that subdomains in the clay grains(agglomerated clay particles) are sufficiently different in water content to give such a profile. Since this profile (at 14.5 mm), to the writer's knowledge, has not been seen by people who have worked on this sample before, it is proposed that this profile has a connection with the humidity gradient which is smaller than what has been the case previously. If this was the case it would strengthen the hypothesis that the intercalation states are highly dependent, and varies according to which local surroundings it "has relaxed into" (in contrast to being only dependent on the macroscopic variable of relative humidity).

The capillary with powder was exchanged with a new sample, and a new humidity gradient was applied, and after about a day, new recordings were made. This was done to have a sharper gradient along the capillary and be more sure that the states which were observed actually was due to random intercalation or potentially not. One new scan is shown in figure 3.2. In this figure a different profile is observed indeed. It is estimated that the capillary is 34 mm from the reservoir of humid air to the reservoir of dry air. The old gradient was approximately two thirds that in magnitude to that of the new capillary. The first gradient's humidity range could have been about $45 - 80\,\%$RH from

the first measuring point to the last one. So the difference was not so big for the humidity gradient, but figure 3.2 shows a situation where the 1WL and 2WL-states are dominating the profile. This is not easily explained, in light of the other profiles, and could be an anomaly.

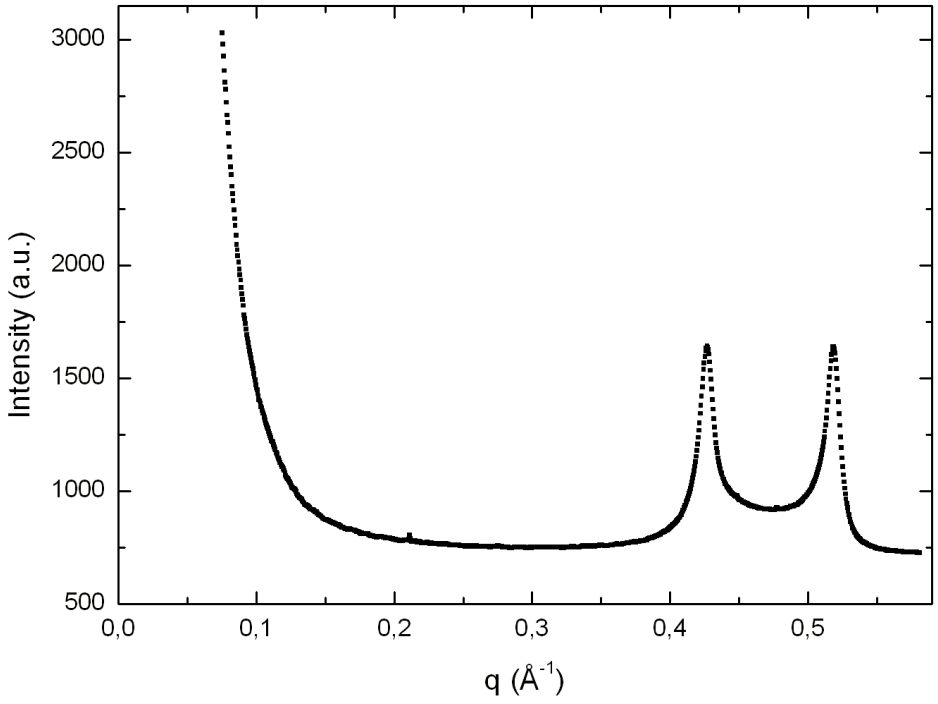

Figure 3.4: A diffraction profile in the capillary showing clear 1WL and 2WL states dominating the diffraction profile.

The beam size for these scans were approximately $200\,\mu$m $\times$ $65\,\mu$m x by y measured as the beam's FWHM. The profile of the beam was elliptical and Bell-curved(Gaussian). Unfortunately for this experiment the beam is more difficult to focus in the x-direction since 5C2 was a bending magnet beamline. This difficulty of focusing in the x-direction comes from the intrinsic divergence of the electron paths being the source. The humidity gradient was along the x-direction. A rough idea of the linkage between the coupling between the gradient and the beam size provides an idea for how much a measured d-spacings can be expected to vary within the beam itself. This argument is not describing the physics of the problem accurately but gives a good idea

of magnitudes. If the humidity gradient amounted to 80 %RH from 0 to 30 mm in the capillary a beam of aforementioned size would map out a region having a difference in relative humidity of about half a procent. Recapitulating the phase transition experiment, it is clear that even such a small difference could be of crucial importance.

Some representative diffraction patterns along the new capillary are shown in figure 3.2. The signatures of mixed intercalation are more

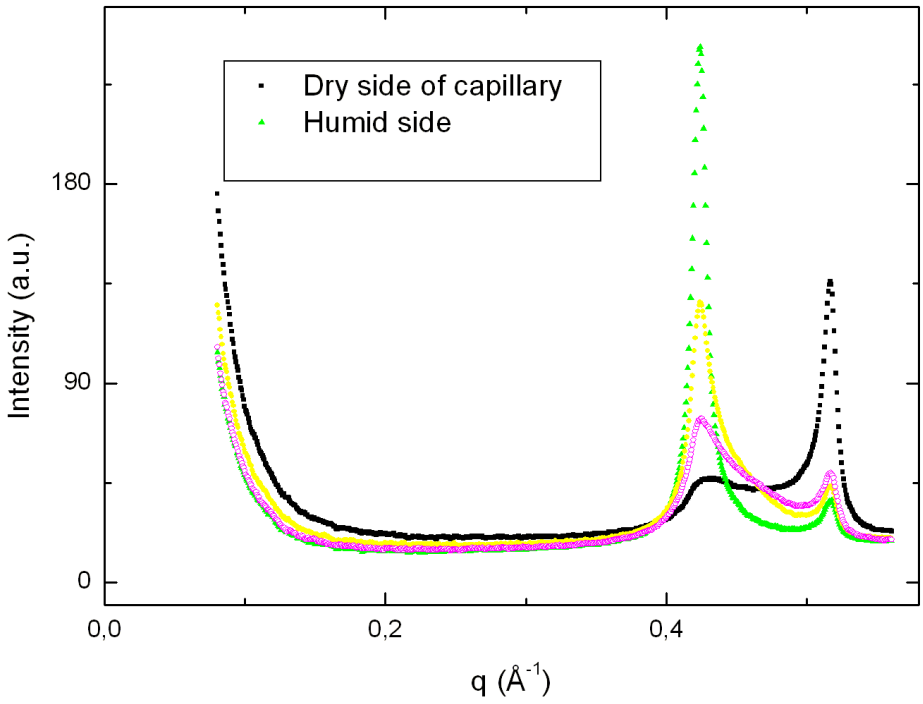

Figure 3.5: Diffraction patterns for the capillary with larger gradient

difficult to locate with the bigger gradient, and it is quite possible that revealing diffraction patterns are lost between data points.

Using smaller beam sizes inadvertently gives a smaller signal since the diffraction volume is made smaller. The diffracton volume will have a square dependence on beam size so going just down to one fourth the beam size in one direction means almost only 5 % of the signal will remain, and that is the ideal case. Since the focusing had to be done mainly by slits at these dimensions, this diminished also the effective source area. The diffraction profile shown in figure 3.2 was

captured with a beamsize of $70 \times 60\,\mu m$.and took more than half an hour to capture. The measuring times for previous scans were about one minute, and have better counting statistics. After the scan in fig-

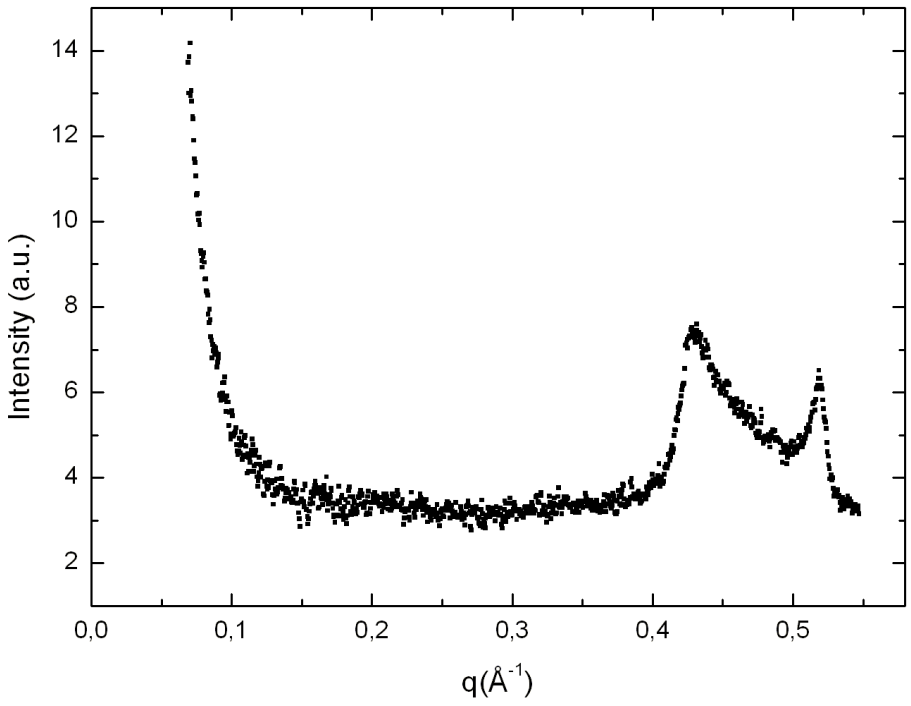

Figure 3.6: A mixed state measured with one of the smallest beam sizes.

ure, which qualitatively was not much different from the previously gathered profiles,(3.2) was finished substantial efforts were put into measuring with even smaller beam sizes, but the very low signal and subsequent noise from the detector (including hot pixels), the measuring times involved and the problems involved in finding the correct place for measuring precluded decisive data on the configuration of mixed-intercalation states in NaFH to be found.

3.3 Wide angle diffraction profile for fluorohectorite

The general goal for the experiment was to gather different diffraction patterns simultaneously testing the detector characteristics. The ex-

periment design was conceptually easy, to hold the humidity constant while heating the sample holder to possibly observe peak shifts for the d(00l)-series and maybe even a phase transition. But although temperature could be effectively changed from $12-60$°C it was not so easy to hold a constant relative humidity. After the frames were recorded a few days after the experiment started the saturated salt solution were not observable any longer in the chamber, even if it was rather moist in the sample cell.

There were small peak shifts during first scans, but it is not known what these exactly should be attributed to. The question is essentially, did the relative humidity or did temperature also induce the shifts? The most likely explanation, from what we have found from comparing two phase transition experiments is that relative humidity alone could explain it. While the temperature is getting higher, the humidity gradient between outside of the chamber and the inside has more potential to be released. The sample cell had been sealed off, but some small openings must have existed of course, for the water to evaporate away.

The stability itself of the relative humidity inside the sample cell, when holding temperature constant,was not compromised to a large effect from the factors mentioned above. So long as the liquid solution with saturated salt still posessed liquid, there would exist an equilibrium state between the production of relative humidity by the salt solution and the transport of water vapor outside induced by a humidity, or pressure gradient. Furthermore, not any substantial differences could be established from scan to scan taken at equal conditions. From the phase transition experiments it was found that equilibrium was reached within 30 minutes for this kind of sample(quite loose powder of relatively small volume).

A diffraction pattern showing one of the frames with best counting statistics is seen in figure 3.3. The (001)-reflection is by far the most dominant in intensity, so the wide angle region is magnified by increasing its intensity sixfold. The $d(002)$ may possibly be detected as a very slight bump, if you know where to look; but is almost totally suppressed by its layer structure factor having a zero in this region. $d(006)$ is probably in the shoulder of the curve with reflections $(130)/(200)$. This diffraction pattern seems to be unordered and a compound of different profiles since multiple peaks in the spectrum are superpositioned. And this is of course due to large sample extension in comparison to the detector dimensions(the sample is in fact only 4cm away). But although some peaks potentially could be better resolved and have sharper spikes given a perfect sample geometry, the widths which comes from the h

and k dimensions in fact will give approximately the profiles seen here. This is in part due to that different Bragg planes with almost the exact same d-spacing comes into a diffraction position([35, 2].

To find the d-spacing for a given (hkl) reflection for the monoclinic cell the following formula can be used (from [20]): $\frac{1}{d^2} = \frac{1}{\sin^2\beta}(\frac{h^2}{a^2} + \frac{k^2\sin^2\beta}{b^2} + \frac{l^2}{c^2} - \frac{2hl\cos\beta}{ac})$.

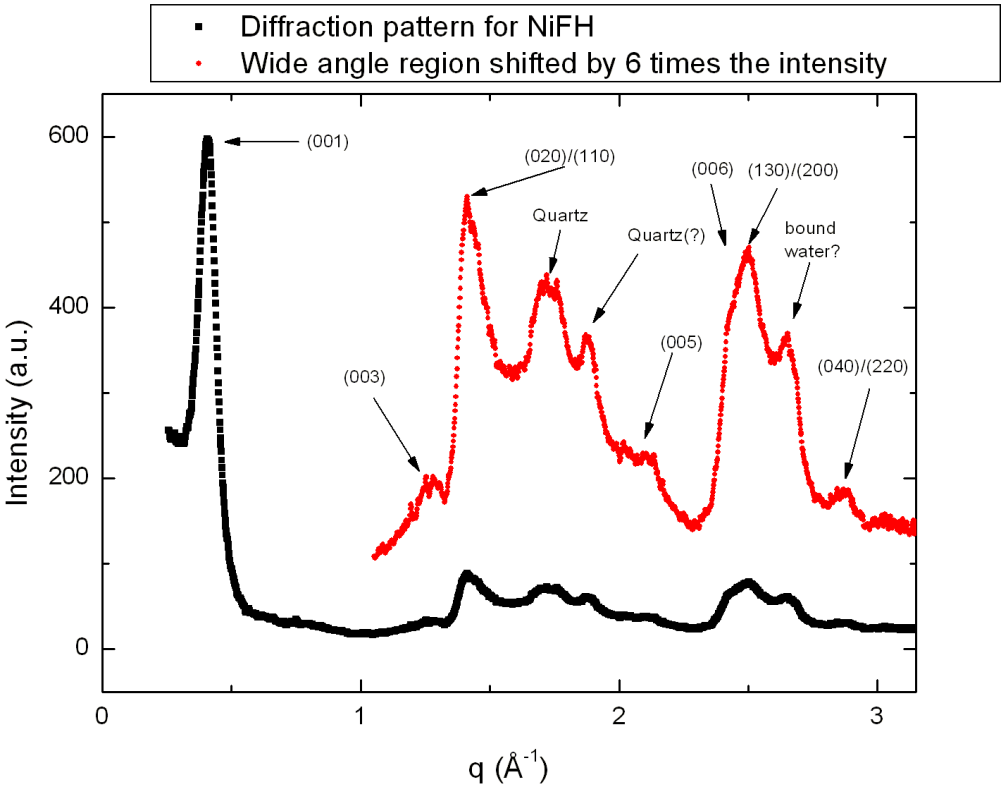

Figure 3.7: NiFH sample at room temperature with a humidity presumed close to 70 %. The $d(001) \approx 15.4$. The identifications is done mostly by comparing to [35, 3, 13], and comparing with previously recorded diffraction patterns from other similar clay samples. The possibly too low signal inbetweeen $d(001)$ and $d(003)$ would come from the subtraction of the kapton window's background which has a diffuse maximum in this region.

The peak labelled in the figure as bound water, the author thinks, is the contribution from an interlayer water molecule bound to both a cation and the silica sheet. And it is not ruled out that also other water molecules bonded in the interlayer should not contribute in this peak.

Other types of bonds could give the same scattering vector, but for the reflection to be appreciable, the bonding should be stable, and not have many different configurations both when it comes to orientations and bond lengths. This would hinder constructive interference. Some details for the profiles near the presumed water bond peak at different d(001) are found in figure 3.3.

It should be realized that the sample broadening, seen in the diffraction profile of figure 3.3, seriously affects its usefulness for calculating different properties of the sample. How exactly it affects the profile can be seen by using a calibration sample with very low intrinsic broadening. For this purpose a SRM Silicon-powder from NIST is used. This profile together with its PseudoVoigtian fit is seen in figure 3.3. Figure

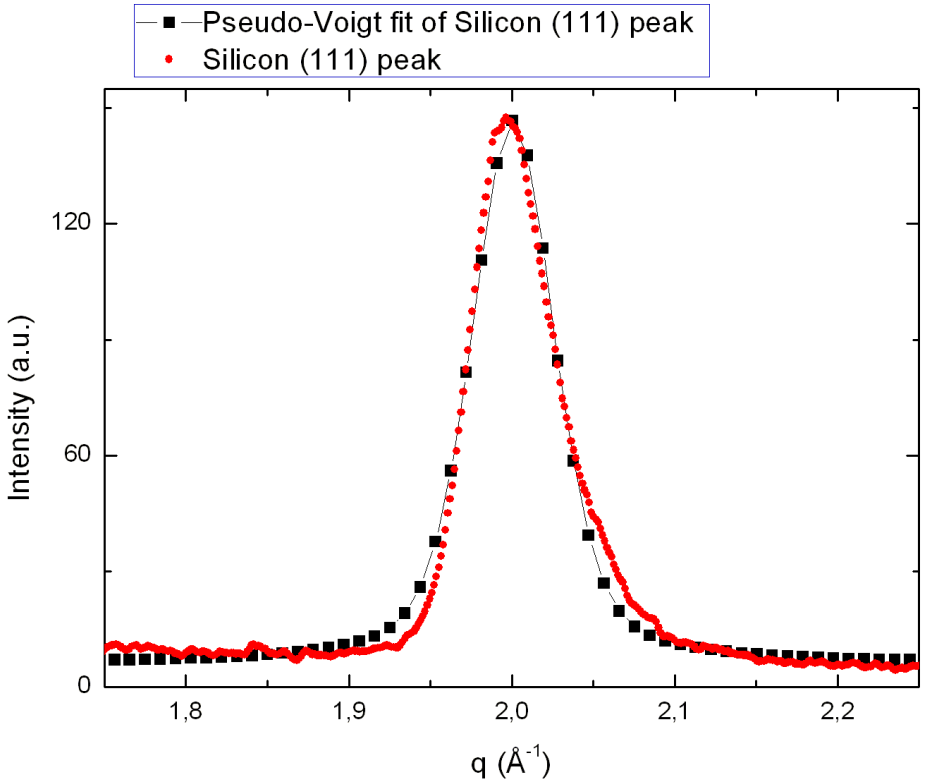

Figure 3.8: The highly asymmetric diffraction profile from the Si-powder used for calibration caused by sample broadening.

3.3 shows the diffraction profile smeared towards higher angles. It is caused by the extension of the sample in space. The contribution from the extension towards the detector will be most important for almost

all practical cases. The part which is hit first by the beam will diffract more than the layers to come, giving a larger contribution to the detected angles at higher angles than the actual diffraction angle, while the lower angles are relatively suppressed. In effect this produces an asymmetry. The extension of the Si-powder calibration sample towards the detector was ≈ 0.3 mm, but the width from the area diffracted could also play a big role. Since the beam size is 0.4 mm or a bit larger than this it should also make a rather large contribution. Diffracting from aluminium foil, of almost negligible thickness, the width of the peak is comparable to those of silicon peaks. This points more to the extension of the beam, than to the thickness of the sample, but there is of course an interplay. Inserting the sample as seen in figure 2.3(b), it was tried to make the powder in the capillary cylinder not sit to far in, as this would cause some of the higher diffraction angle to be stopped by the copper. Of course the experimenter did his best, but balancing this requirement, and at the same time trying to limit the thickness of the powder to 1 mm proved quite challenging and it can not be guaranteed that the the intensity at higher angles might be relatively smaller than it should have been. As an effect of broadening effects, which are angle dependent, and difficult calibration procedures, it precludes from reliably doing most quantitative analysis. Therefore, only d-spacings and qualitative asessments of peak shapes will be handled in the further discussion

The peak labelled as bound water, the author thinks, is interlayer water bound to both cations and the silica sheet. Possibly it could come from adsorbed water on the clay surface as well. And it is not ruled out that also other water molecules bonded in the interlayer should not contribute in this peak. Other types of bonds could give the same scattering vector, but for the reflection to be appreciable, the bonding should be stable, and not have many different configurations both when it comes to orientations and bond lengths. This would hinder constructive interference. Some details for the profiles near the presumed water bond peak at different d(001) are found looking into figure 3.3.

In figure 3.3 the dependence on the d-spacing will briefly be discussed. From [21] the "2WL state" for NiFH is known to be at 15.9 [2]. A "1.5WL" corresponds to 14.5 Å, and a "1WL" to 13.7 Å. Two qualitatively different behaviors can be distinguished. The three first curves, black, red and green have d-spacings near eachother and all have something resembling a plateau where the line is drawn. The other curves, except the last one, have on the contrary a peak in the region. In an

[2] This d-spacing corresponds to a not so stable state, and a so-called 1.5WL is probably more stable[12, 14].

article by Skipper et.al.[22] where hydrated Ni-Vermiculite is studied by neutron diffraction in conjunction with substitution of H2O by D2O they found that water molecules are quite strongly attached to the clay, and that one peak from such ordering was from the hydrogen atoms on the water molecules facing the clay. The peak's position was at 2.4 . and corresponds to the distance between the Ni-cation and the hydrogens. Since Ni-Vermiculite is a very similar clay to NiFH, the most important difference being the layer charge, it is plausible that the peak observed in this report should be understood down the lines proposed in this report. But it may seem strange that the pronounced peaks occurs at lower humidity rather than higher humidities, but it is proposed that this is caused by more order in the hydration states of lower humidity. The hydration of the cations may take forms not favorable for fitting the solvation shell into the interlayer. This will as a concequence cause less structural ordering in the interlayer.

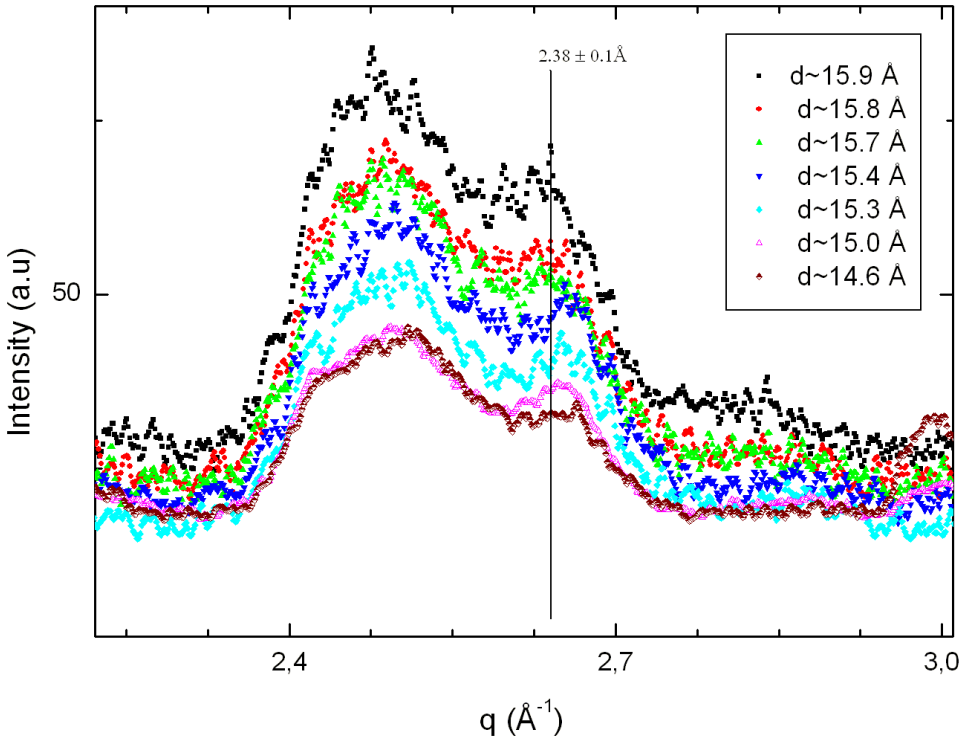

Figure 3.9: Different peak profiles at different $d(001)$ at a presumed water bond peak. The interesting feature to look for is the flattening out to a plateau or a small but distinct peak at the position of or a bit beyond the indicated line giving the d-spacing for this q-value. This qualitative difference between different intercalation states gives reason to believe that this could be due to water bonding. The two lowest curves have the lowest noise in the signal since these actually have much more counts than the other curves.

Chapter 4

Conclusions

Phase transitions in NaFH, water bonding in the NiFH interlayer and HT-states in NaFH have been studied in this report. Naturally the data is much richer than the analysis presented have taken account for. But it is quite certain that the physical system(a hydrated powder sample) under study have been disordered at scales of macropores, down to the molecular scale of bonding in the interlayer. As there is a complex interplay of factors between the different lengthscales and phenomenons all of the diffractograms information could not be interpreted unambigously. Notwithstanding this cautionary note the main conclusion is that disorder exists between layers in NaFH-particles resembling HT-states. It will not be concluded from what effect this mixed intercalation stems from, but a nontrivial[1] dependence of a water content gradient in micropores is conjectured.

Furthermore evidenced from the different experiments is the heterogeneity of hydrated intercalation states in NaFH. Over a quite large range of RH different intercalation states are found. This means, in part, that particles don't switch from one state of hydration to the other, but that they would possibly undergo many states of mixed intercalation adopting more interlayers with 2WL as hydration progress. Given the predominance of either a 1WL or 2WL peak in most diffractograms, also under small hydration/temperature gradients, a fully random intercalation is not likely to happen in the NaFH-particles. It is conjectured that there exists a dependence of water layer state of one interlayer to the previous one in the layer stacking. A physical explanation for such an effect could come from the particles in the interlayer negotiating with the clay layer in a way to prefer a similar stacking in the next interlayer, or it could stem from the way the layers are stacked

[1] Nontrivial in the meaning that the beam is relatively small enough not to map out a volume of big water content difference.

onto eachother creating domains energetically favoring relatively one kind of hydration state to the other. A third explanation could be that the layers experience different environments on the exterior of the particle. This last possibility, is not deemed likely to explain the dependency though by the author trying to imagine such environmentsidea, but the boundary conditions, as they are, will of course play a crucial role in determining prevalent hydration states.

Suggestions for further work

It should be possible to manipulate humidity gradients, sample geometry and beam size in certain ways to see how this changes diffraction patterns. This would give some conclusions and new conjectures on deciding mechanisms behind mixed intercalation and HT-states in NaFH.

Further work on WAXS patterns of fluorohectorite should focus on sample geometry, calibration and minimizing sample broadening if the 'Nanostar' is utilized. For qualitative data on shapes and profiles the 'Nanostar' X-Ray diffraction setup may be utilized, but data for quantitative analysis would best be done on instruments designed for a constant sample to detector distance at wide angles.

Appendix A

X-Ray microscopy images of NaFH-particles

At PAL, Korea, an X-ray beamline with a pre-configured setup was utilized to make images of clay particles of NaFH.

Hwa Shik Youn, the responsible scientist for the X-ray microscope, took the images and provided membranes onto which the particles could be suspended.

Sample preparation

A small amount of clay particles of the type NaFH(Sodium-Fluorohectorite) were dispersed in deionized water, a very small drop of the solution was carefully placed on top of a membrane of Silicon nitride with thickness of 20 μm. When the drop had completely evaporated the sample was ready for being measured.

Imaging technique and instrument characteristics

For the images recorded the setup was made as in figure (A) using a Zernike phase contrast. This allowed better resolution than a bright field image[40] but produces a Halo effect, overemphasizing density variations.

One of the big advantages of the X-ray microscope is that it has an in depth view, but this is effective only to about 100 μm before the sample is too absorbing for good images to be taken for samples with typical absorption coefficients. The settings of the instruments while imaging clay particles was the maximum magnification giving pictures of $20 \times 20\,\mu$m in size, necessitating moving the sample to view over all of the membrane's area. The resolution can be seen in figure (A)

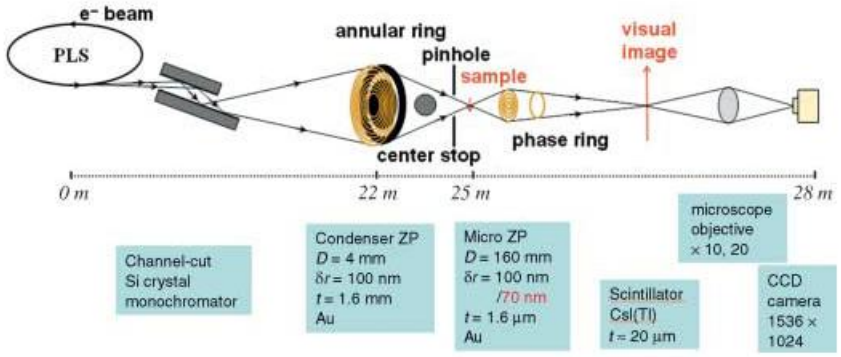

Figure A.1: The principal setup for the optical system is displayed. The figure is taken from [40]. The Fresnel zone plate focuces a monochromatized beam onto the sample and a micro zoneplate brings out the phase dependencies and the image formed can be magnified and seen with a CCD-camera.

,which is a frame from a test sample, to be about 80 nm(The vertical lines have a width according to the ruler shown),

Data

One more or less typical image is shown first in large dimensions. The image has different regions where different patterns are seen. In the center and the bottom middle sections are shapes very much resembling that of clay particles, and having the dimensions also indicating it should be that. For the structure having the ruler next to it in the middle, there is a darker region in the middle, and seems to have two distinct parts which make a compound structure. Since the overlap region is darker, it is justified to think that this structure is made up of two seperate particles joined to eachother. The region to the left could possibly be a quite many particles on top of eachother to make piled structures resembling cliffs or mountains. The areas of sharp white stemming from the halo effect inbetween the dark areas support the notion that these are cliff-like structures. It is proposed that the NaFH-particles here may be preferentially aligned with layers perpendicular to the surface of the membrane.

As may be investigated by the reader her- or himself the particles seen in the previous image is not the only particlesize showing up in the images. Some particles seem to have lengths of at least 5 μm.

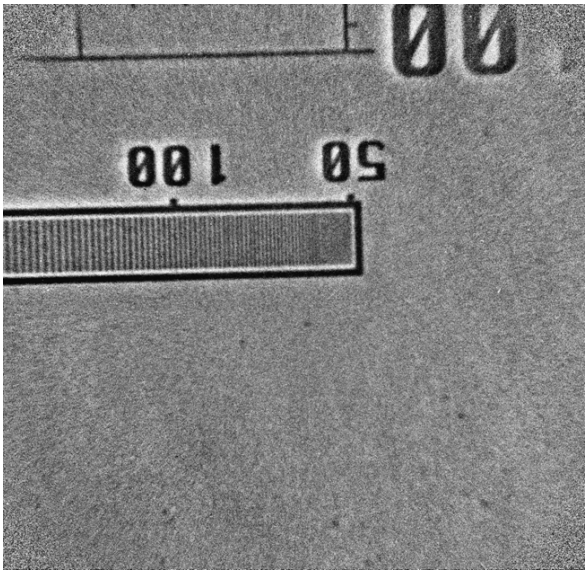

Figure A.2: The test sample providing the resolution.

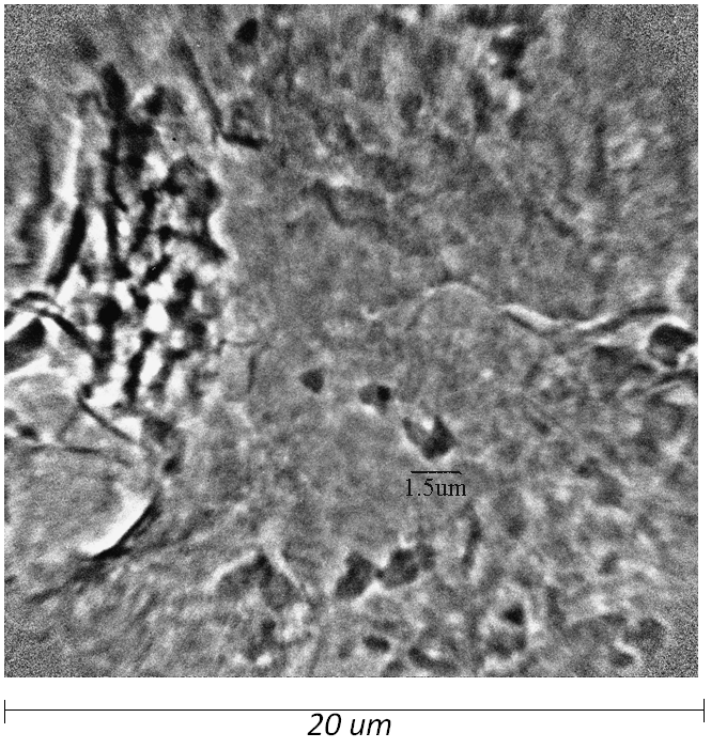

Figure A.3: One image magnified and scales shown.

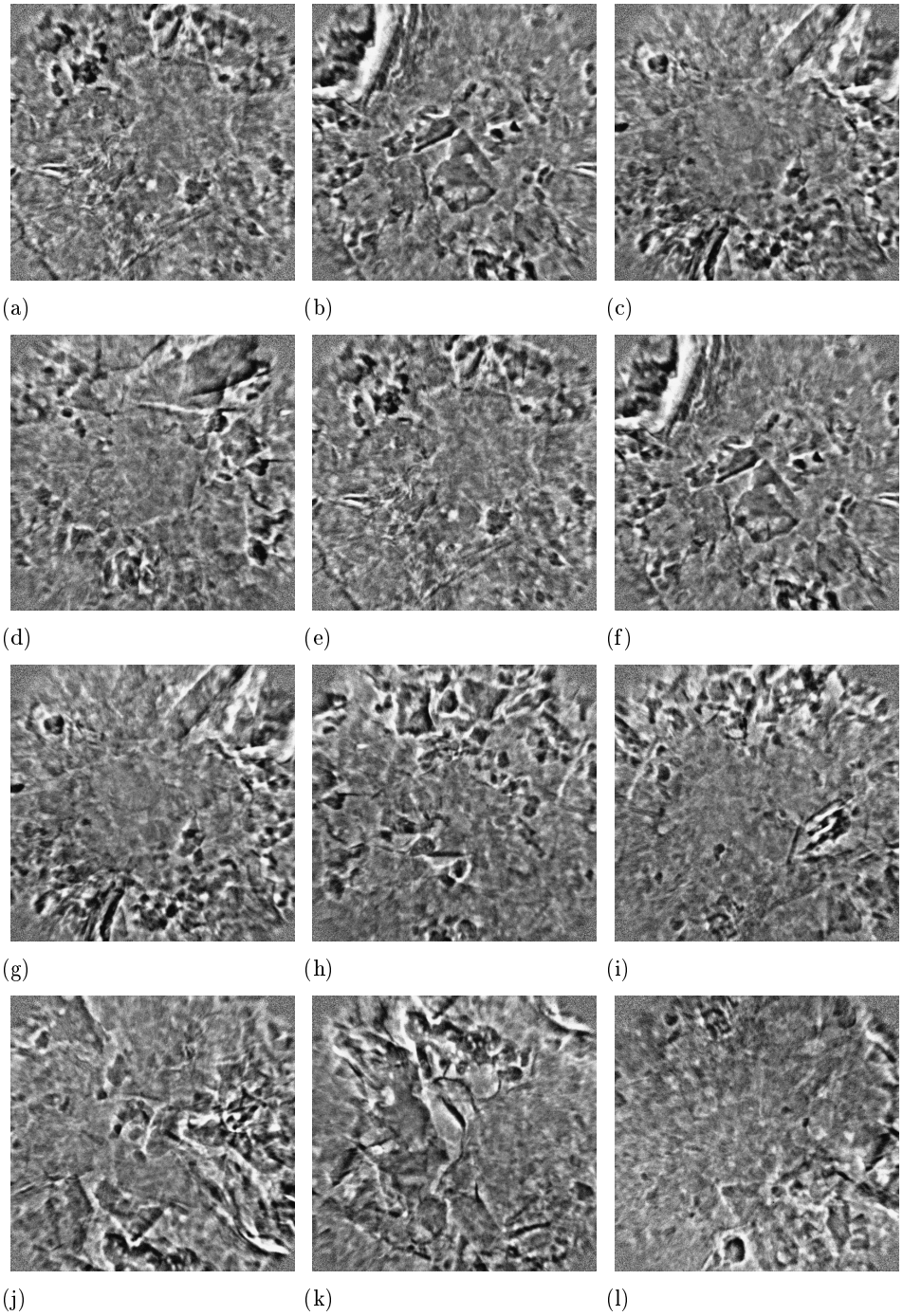

Figure A.4: One collection of the images taken

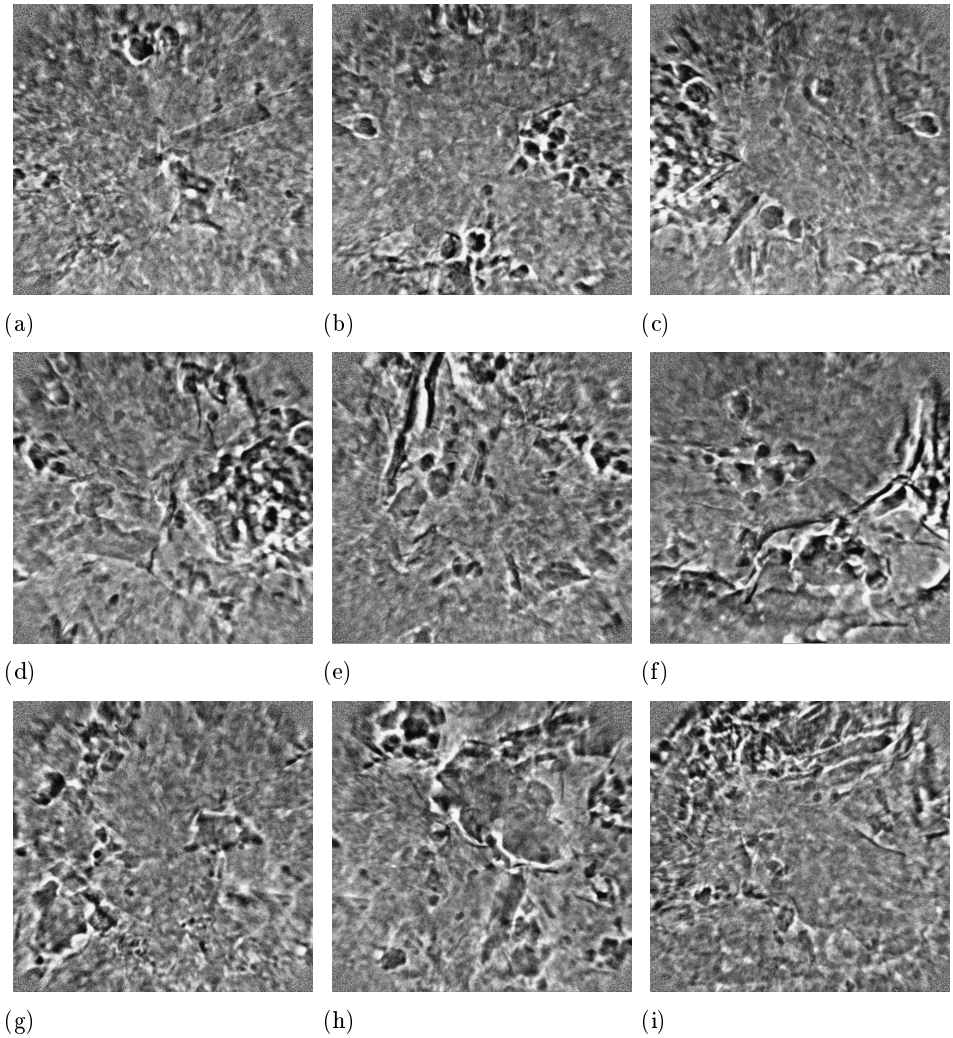

Figure A.5: The last frames collected

Bibliography

[1] "mineral" *Encyclopdia Britannica.* 2007, Encyclopdia Britannica Online. 11 Mar. 2007 <http://search.eb.com/eb/article-9109683>.

[2] Moore, M. D.;Reynolds,R. C. *X-Ray Diffraction and the Identification and Analysis of Clay Minerals* 1989, Oxford University Press

[3] da Silva,G. J.; Fossum,J. O. et al. *Synchrotron x-ray scattering studies of water intercalation in a layered synthetic silicate* 2002, Physical Review E 66

[4] Internet source, *Materials chemistry*, URL: <http://www.materialkemi.lth.se/ Lund University>, Sweden (2006)

[5] van Olphen, H. *An Introduction to Clay Colloid Chemistry* 1977, John Wiley & Sons

[6] Woolfson, M. M *An Introduction to X-Ray Crystallography* 1997, Cambridge University Press

[7] Elliott, S. *The Physics and Chemistry of Solids* 1998, John Wiley & Sons

[8] Eberl, D. D.; Srodon, J. et al. *Otwald Ripening of Clays and Metamorphic Minerals* 1990, Science Vol. 248

[9] Vaia, R. A.; Liu, W. *X-Ray Powder Diffraction of Polymer/Layered Silicate Nanocomposites: Model and Practice* 2002, Journal of Polymer Science

[10] Alme, L. R. *Water transport in selected nanoporous media* 2007, Master's thesis, NTNU

[11] Hølto, J. *Experimental Studies of a Layered, Synthethic Silicate:TGA, DSC and X-Ray Scattering* 2007, Master's thesis, NTNU

[12] Fischer, A. *Water penetration and intercalation: A neutron and x-ray study of fluorohectorite* 2007, Master's thesis, NTNU

[13] Dagois, S. *A thermogravimetric- and X-ray scattering- study of hydration transitions in a nano-layered silicate synthetic clay*, 2005, NTNU

[14] Kjelling, B. M., *Water intercalation in Nickel Fluorohectorite* 2007, Project work NTNU

[15] Heidolph Instruments *Instruction Manual Pump drive* Heidolph Instruments GmbH & Co.KG

[16] Vaisala *HMI38 Humidity Data Processor, Operating Manual* 1995

[17] Postech *Pohang accelerator laboratory* URL:<http://paleng.postech.ac.kr/>, 2008

[18] Wexler, A. *Humidity and Moisture* 1965 Vol. 3 Fundamentals and standards, Nationalal Bureau of Standards, Reinhold publishing corporation

[19] Greenspan, L. *Humidity Fixed Points of Binary Saturated Aqueous Solutions* 1977, Journal of research of the National Bureau of Standards-A

[20] Cullity, B. D. and Stock, S. R. *Elements of X-ray diffraction* 2001, Prentice Hall

[21] Aalerud, T. N. *Synchrotron X-ray Scattering Studies of Water Intercalation in Synthetic Nickel-Fluorohectorite* 2001, Master's thesis, NTNU

[22] Skipper, N. T.; Soper et al. *The Structure of Interlayer Water in a Hydrated 2:1 Clay* 1989, Chemical Physics Letters Vol 2, 166

[23] Breu, J.; Seid, W.,Senker,J.; *Synthese von dreidimensional geordneten Einlagerungsverbindungen des Hectorits* 2003, Zeitschrift fr anorganische und allgemeine Chemie

[24] Princeton Instruments *PIXIS-XF:1024F*URL: <http://www.piacton.com/products/xraycam/pixisx/default.aspx>, 2008

[25] Thompson, A. C. and Vaughan, D. *X-Ray Data Booklet* 2001, Lawrence Berkely National Laboratory

[26] Edited by Brauchel,J;Hodeau,J.L., Lehmann, M.S. et al. *Neutron and synchrotron radiation for condensed matter studies* 1993, Les Editions de Physique, Springer Verlag

[27] Breu, J.;Seidl, W. et.al. *Charge homogeneity of synthetic fluorohectorite* 2001, Chemistry of materials

[28] Guinier, A. *X-Ray Crystallographic Technology* 1952, Hilger and Watts Ltd.

[29] Hendricks, S., Teller,E. *X-Ray Interference in Partially Ordereed Layer Lattices* 1942, The Journal of Chemical Physics

[30] IUCr, Crystallographers online *Half a century of synchrotron radiation* http://www.iucr.org/cww-top/his.sync50.html May 1997, *From CERN Courier*

[31] Suzuki, M.;Wada,N. et.al. *Hydration states and phase transitions in vermiculite intercalation compounds* 1987, Physical Review B

[32] Vömel, H. *Saturation vapor pressure formulations* 2006, <http://cires.colorado.edu/ voemel/vp.html> CIRES, University of Colorado

[33] Sourceforge URL: <http://yorick.sourceforge.net/index.php> Developed at MIT

[34] Løvoll, G., Sandnes, B. *Dynamics of water intercalation fronts in a nano-layered synthetic silicate: A synchrotron scattering study* 2005, Physica B

[35] Brindley, G. W.;Brown, G. (Editors) *Crystal Structures of Clay Minerals and their X-Ray Identification* 1980, Mineralogical Society

[36] Thompson, P.; Cox, D. E. and Hastings, J. B. *Rietveld Refinement of debye-scherrer synchrotron x-ray data from* $Al_2{=}_3$ 1987, J. Appl. Chryst. 20

[37] Wertheim, G. K.; Butler, M. A. et al. *Determination of the gaussian and lorentzian content of experimental line shape* 1974, Rev. Sci. Instrum. 45 (11)

[38] Bruker AXS *NanoSTAR SAXS System User Manual* Vol. 2, 2004

[39] Knudsen, K. D.; Fossum ,J. O. *Pore characteristics and water absorption in a synthetic smectite clay*

[40] Youn, H. S.; Jung, S. W. *Hard X-ray microscopy with Zernike phase contrast* 2006, Journal of Microscopy